Science Advances
AAAS

Supplementary Materials for

Single-cell multi-omics sequencing uncovers region-specific plasticity of glioblastoma for complementary therapeutic targeting

Xin Wang *et al.*

Corresponding author: Liang Chen, chenliang8@genomics.cn; Baohui Liu, bliu666@whu.edu.cn; Ying Gu, guying@genomics.cn

Sci. Adv. **10**, eadn4306 (2024)
DOI: 10.1126/sciadv.adn4306

The PDF file includes:

Other Supplementary Material for this manuscript includes the following:

Materials and Methods

Patient sample collection

The tumor core and paired peritumoral brain tissues were collected from patients with GBM during the surgery performed in the Department of Neurosurgery, Renmin Hospital of Wuhan University, China. The detailed information of each patient was provided in table S1. To ensure the high quality for downstream library construction, collected tissues were placed in liquid nitrogen within 15 minutes after resection. GBM was preliminarily diagnosed by computed tomography (CT) or MRI, and later confirmed independently by three neuropathologists in the Department of Pathology at Renmin Hospital of Wuhan University via the post-operative histopathological examination. Particularly, the mutational status of isocitrate dehydrogenase (*IDH*) for each tumor sample were assessed via immunohistochemistry and/or DNA sequencing.

Hematoxylin-eosin (HE) staining

By following the standard protocol of HE staining, tissue sections were stained in the hematoxylin solution for 5 minutes and then washed by running water at room temperature for 5 minutes. Subsequently, the tissue slides were dyed with the eosin solution for 2 minutes, and were then gradually dehydrated by treatment of an increasing concentration of ethanol (75%, 95%, and 100%). Finally, the slices of HE staining were visualized using a slide scanning system (Axio Scan.Z1, Zeiss, Germany).

Preparation of single cell nucleus suspension

Single nuclei were prepared as previously described (*115*). All the following processes were carried out on the ice except for other description. Briefly, tissue was thawed and cut into small pieces in a culture dish. Then, those small pieces were transferred to a 2 mL Dounce tissue grinder (Sigma) with 2 mL of homogenization buffer containing 500 mM sucrose (Sigma), 20 mM Tris pH 8.0 (Thermo Fisher Scientific), 10 mM $MgCl_2$ (Thermo Fisher Scientific), 50 mM KCl (Thermo Fisher Scientific), 1× protease inhibitor cocktail (Roche), 0.1% NP-40 (Roche), 0.1 mM DTT, and 1% nuclease-free BSA. Five minutes later, tissue was first homogenized by 15-20 strokes of the dounce pestle A (loose), and then the 15-20 strokes of the dounce pestle B. The homogenate was subsequently collected and filtered into a 15 mL centrifuge tube through a 70 μM cell strainer (BD) and a 30 μM cell strainer (SYSMEX PARTEC). Then, the filtered homogenate was centrifuging at 500 g for 5 minutes at 4°C. The supernatant was discarded and the pellets were resuspended and counted with DAPI.

Construction and sequencing of snRNA-seq library

snRNA-seq library was prepared with the kit of the DNBelab C Series Single-Cell Library Prep Set (MGI) as described previously (*34*). Briefly, snRNA-seq libraries with the barcode were constructed from the single-cell suspensions through following steps, including encapsulation of droplet, emulsion breakage, collection of mRNA captured bead, reverse transcription-polymerase chain reaction (RT-PCR), amplification and purification of cDNA. The protocol of manufacturer was also applied to construct indexed sequencing libraries. Then, Qubit ssDNA Assay Kit (Thermo Fisher Scientific) was used to assess the quality of the sequencing libraries before they were sequenced by the machine of DIPSEQ T1 sequencer (BGI). Paired reads were sequenced. Read 1

contained 10 bp unique molecular identifier (UMI), 10 bp cell barcode 1, and 10 bp cell barcode 2. Read 2 contained 10 bp sample index and 100 bp transcript sequence.

Construction and sequencing of snATAC-seq library

snATAC-seq library construction was performed as described by Yu et al (*116*). Briefly, the kit of DNBelab C Series Single-Cell ATAC Library Prep Set was used to construct single-nucleus ATAC-seq library. snATAC-seq libraries with the barcode were converted from transposed single-nucleus suspensions, through steps as follows: encapsulation of droplet, pre-amplification polymerase chain reaction, beads emulsion breakage, beads collection, DNA amplification, and purification. Indexed sequencing libraries were prepared according to the protocol. Qubit ssDNA Assay Kit (Thermo Fisher Scientific) was used to assess the quality of sequencing libraries before sequencing, and a paired-end 50 sequencing scheme was used by DIPSEQ T1 sequencer (BGI).

Analysis of snRNA-seq data

snRNA-seq data preprocessing

The raw reads after sequencing were parsed and cell barcodes were corrected by PISA software (version 0.7) (*117*). Then the clean reads were aligned to GRCh38 (hg38) genome by STAR software (version 2.7.9a) (*118*), and the obtained SAM files were transformed to BAM format files. After sorting of BAM files, empty droplets were filtered by R package DropletUtils (*119*), and the resulted cell expression matrixes were generated by PISA.

Then, Seurat (version 4.0.5) (*120*) and DoubletFinder (version 2.0.3) (*121*) were applied in the following analysis. First, the Seurat objects were generated based on the above matrixes and high-quality cells were acquired through three criteria: 1) genes expressed in more than 5 cells and cells with detected genes more than 500; 2) cells with mitochondrial genes expression proportion less than 5%; 3) cells without extreme outliers of the number of detected genes. Next, doublets were filtered out by DoubletFinder according to the threshold of 5%. After the above preprocessing, matrixes from different samples were merged by Seurat for cross-sample comparison in the following analysis. Particularly, the merged count matrixes were log-normalized by 'NormalizeData' function and scaled by 'ScaleData' function. Then, the 3,000 most variable genes were identified by 'FindVariableFeatures' function and principal components (PCs) were calculated by 'RunPCA' function. Nearest neighbors were computed based on the top 30 PCs, and then 19 clusters were identified by 'FindClusters' function (resolution = 0.6). Finally, uniform manifold approximation and projection (*122*) implemented in Seurat was used to embedding cells onto two-dimensional graphic.

Cell type annotation

Annotation for each cluster was manually performed based on the expression of canonical marker genes. The marker genes used were *EGFR, PTPRZ1* (GBM cell); *TPD52L1, ALDOC, CLDN10, ETNPPL* (Astrocyte); *PLP1, MOG, MOBP, CLDN11* (Oligodendrocyte); *GAD2, GAD1, SLC32A1* (Inhibitory neuron); *SLC17A7, NRGN, NEUROD2, NEUROD6* (Excitatory neuron); *APBB1IP, CD74, C1QA* (Myeloid); *CD2, CD3D, CD3G* (T cell); *MCAM, CLDN5* (Pericyte/endothelial cell).

Differential expressed genes analysis

DEGs for each cell type were identified by 'FindAllMarkers' function in Seurat, the expression of one cell type was compared with the rest cell types. Wilcoxon statistical test was employed. Particularly, avg_log2FC > 0.5 and *p* value < 0.05 were used as the criteria to filter the DEGs.

CNVs and phylogenetic tree analyses

To identify malignant cells from the samples, the CNVs of each cell were estimated with the inferCNV package (version 1.8.1) (*28*). To obtain accurate CNV results accurately, we implemented the inference process for every patient separately and used their normal cells (microglia and oligodendrocytes) from corresponding peritumoral brain as reference cells. In this analysis, the parameters used include: cutoff = 0.1, cluster_by_groups = T, analysis_mode = 'subclusters', HMM = T, tumor_subcluster_partition_method = 'random_trees'. After CNVs were obtained, we employed *k*-means clustering to group cells based on the CNV pattern and visualized the CNV results on heatmap generated by the ComplexHeatmap package (version 2.11.1) (*123*). To guarantee the accuracy for identifying malignant cells, only cells containing chr7 amplification and chr10 deletion simultaneously were judged as malignant cells.

Based on the CNV location on chromosome, each p- or q-arm level change was converted to equivalent CNV by consulting the information of the genomic cytoband, and each CNV was further annotated as gain or loss. Finally, the evolutionary tree was constructed by the arm level of CNV and subclones containing identical ones were collapsed. UPhyloplot (version 2.3) (https://github.com/harbourlab/uphyloplot2) (*47*) was used for data visualization.

GO enrichment analysis

The clusterProfiler (version 4.0.5) (*124*) R package was applied to obtain the enriched GO terms (biological processes). The enriched terms were filtered by setting qvalueCutoff = 0.05, and were then visualized by ggplot2 (version 3.3.5) (https://github.com/tidyverse/ggplot2) R package.

Prediction of the transcription factor regulatory network

The pyScenic (versions 0.11.2) (*62*) software was used to identify the transcription factor regulatory networks. The GRCh38 version of reference files were used, and default parameters were applied. This prediction process consists of three steps: 1) 'pyscenic grn', which identifies TF and its target genes, named a regulon, based only on the expression profile of the cell; 2) 'pyscenic ctx', which simplifies the regulon and removes the target genes without the motif corresponding to the TF. 3) 'pyscenic aucell', the Area Under the recovery Curve (AUC) of the genes was measured to define the regulons based on the enrichment of the previously identified regulons.

Subpopulation analysis of GBM cells

After annotation for cell types, GBM cells were extracted and then subdivided into sample-specific objects by 'SplitObject' function in Seurat. For the GBM cell objects, the 'SelectIntegrationFeatures' function was used to select the genes that are repeatedly variable across datasets, and then anchors among the objects were called for integration by 'FindIntegrationAnchors' function. Subsequently, the different GBM cell datasets were integrated by 'IntegrateData' function and subclustered by "FindClusters" function.

Pseudo-time trajectory analysis

To construct the pseudo-time trajectory for GBM cells, the Monocle package (version 2.18.0) (*82*) was applied. The highly dispersion genes among the extracted cells were identified to arrange the

cells on two-dimensional plot. After the trajectory was constructed, genes changing with the trajectory were identified by 'differentialGeneTest' function and the significantly altered genes (*q* value < 1e-4) were selected for downstream analyses. The changes of selected genes along different branches were analyzed by "BEAM" function, and patterns of these genes were further visualized by "plot_genes_branched_heatmap" function.

RNA velocity analysis

RNA velocity (transcriptional dynamics of splicing kinetics) of selected cells was used to deduce the transition status of cells. First, we used velocyto (version 0.17.17) (*125*) to obtain the ratio of its spliced- and unspliced- messenger RNA (mRNA). Then, scVelo (version v0.2.4) (*83*)was used to analyze the state transition. In details, velocities were calculated by setting the parameter: mode = 'deterministic', and the obtained velocities are vectors in gene expression space, representing the direction and speed of movement of the individual cells. Then, the velocities were projected onto the embedding graphic.

Analyses of snATAC-seq data

snATAC-seq data preprocessing

The raw paired-end sequencing data of snATAC-seq were parsed and adapter sequence were trimmed by PISA, and the processed data were then aligned to GRCh38 (hg38) genome by bwa (*126*). Bap2 (https://github.com/caleblareau/bap) was used to deconvolute the beads, beads from the same droplet were combined according to their index. After the alignment and combination, fragment files were obtained.

ArchR (version 1.0.1) (*127*) was used to perform the following analysis with the obtained fragment files. First, for each sample, low-quality cells were filtered out. Particularly, the parameter minTSS was set as 4, minFrags as 1000, and maxFrags as 100000. To remove the doublets from the samples, the built-in function 'addDoubletScores' was applied and the parameter filterRatio was set as 2. After the data were preprocessed, 'addIterativeLSI' was performed for dimension reduction, and the key parameters were: resolution = 0.2, sampleCells = 10000, varFeatures = 25000, dimsToUse = 1:30. We did 'addClusters' function to cluster cells and 'addUMAP' function was used for embedding.

Cell annotation and peak analysis

To annotate the cell clusters in snATAC-seq, we considered the results from three strategies: 1) the chromatin accessibility around the canonical marker genes mentioned in above section; 2) the gene activity score inferred from the openness of the marker genes and the corresponding promoter region; 3) the cell types predicted from the integration with the gene expression matrix of snRNA-seq.

Based on ArchR's built-in functions, peak identification, motif annotation, peak-to-gene analysis, and co-accessibility analysis were accomplished by 'getMarkerFeatures', 'addMotifAnnotations', 'addPeak2GeneLinks', and 'getCoAccessibility' function respectively. In peak-to-gene analysis, the key parameters include: maxDist = 250000, scaleTo = 10^4, log2Norm = TRUE, and predictionCutoff = 0.4, which are specified in 'addPeak2GeneLinks'. Similarly, the parameters corCutOff = 0.45, FDRCutOff = 1e-04, varCutOffATAC = 0.25, and varCutOffRNA = 0.25, pertaining to peak-to-gene analysis, are set within the 'plotPeak2GeneHeatmap' function.

Identification of malignant cells

In snATAC-seq, the R package Copy-scAT(*35*) was employed to identify malignant cells. The input was the fragment format file. The procedure includes three steps: 1) fragment pileup and normalization; 2) chromosome arm CNV analysis; 3) detection of amplifications. Particularly, only barcodes with a minimum number of 5000 fragments were retained, and a pileup of total coverage (number of reads × read lengths) over bins of 1 Mbp was generated. To account for differences in read depth, binned read counts were linear normalized over the total signal in each cell, and chromosomal bins that consist predominantly of zero were filtered out for further analysis.

Function enrichment of cis-regulatory elements

GREAT (*40*) was applied to perform the functional enrichment analysis for cis-regulatory regions identified in snATAC-seq. Particularly, differentially accessible distal peaks for each cell type were supplied to GREAT and the curated GO terms (biological process) were chosen for enrichment with the binomial FDR value. The resulted terms were visualized by heatmap generated using scanpy(*128*).

Assignment for GBM cells to cellular states

The cellular states of GBM cell were identified by the expression score for four state modules (MES-like, NPC-like, AC-like, and OPC-like) according to the method described in previous study(*22*). In detail, the signatures of each cellular state were obtained from Neftel et al. (*22*). Particularly, signatures for MES1-like and MES2-like were grouped into MES-like. Similarly, the NPC1-like and NPC2-like were grouped into NPC-like. The average expression of the obtained signatures for each GBM cell were calculated for assigning the cellular states. The state results were visualized using ggplot2, with each position representing their relative expression score and each quadrant corresponds to specific cellular states.

Cell lines and cell culture

Human glioblastoma cell lines U251, and mouse glioma cell line GL261 were purchased from the Cell bank of Chinese Academy of Science (Shanghai, China). Cells were cultured in DMEM supplemented with 10% fetal bovine serum (Gibco, USA) and 1% penicillin-streptomycin and were kept in a humidified 5% CO_2 incubator at 37°C.

Cell transfection

Plasmids of pLVX-CMV-fluc-puro, pMD2.G and psPAX2, pCDNA3.1-Flag-BACH1, and specific shRNA targeting of human were obtained from Miaoling Biology (Wuhan, China). shRNA targeting of mouse *Bach1* was purchased from Genechem (Shanghai, China). For stable cell line (U251-shBACH1 and GL261-shBach1-Luc) construction, lentivirus was produced in 293T cells helped with lentivirus packaging plasmids (pMD2.G and psPAX2). Transfections were helped with Lipofectamine 3000 (L3000015, Thermo Fisher Scientific) in accordance with the manufacturer's protocol. The specific sequence of shRNA targeting of U251 (shBACH1) is GATGTGCTGTGCGATGTCACC and the sequence of shRNA targeting GL261 (shBach1) is GCTCGACTGTATCCATGACAT.

Reagents and antibodies

Ulixertinib (an inhibitor of ERK1/2, S7854) and hemin (protohemin, an inhibitor of BACH1, S5645) were purchased from Selleck (USA).

The antibodies and their dilutions used in this research were as follows: anti-GAPDH (1:3000, 5174, Cell Signaling Technology), anti-BACH1 (1:1000, 14018-1-AP, Proteintech), anti-ERK1/2 (1:1000, 4695, Cell Signaling Technology), anti-Phospho-ERK1/2 (1:1000, 4370, Cell Signaling Technology), anti-Vimentin (1:2000, 10366-1-AP, Proteintech), anti-N-cadherin (1:1000, 22018-1-AP, Proteintech), and anti-cleaved caspase 3 (1:1000, ab32042, Abcam).

Western blot analysis

Cells were lysed in RIPA Buffer (Servicebio, China) supplemented with a phosphatase inhibitor Cocktail (Roche, Switzerland). Protein concentration was quantified using a BCA Protein Assay Kit (Beyotime, China). 10 μg of protein was separated on SDS-page and transferred to PVDF membrane (Millipore, USA). After blocking in nonfat milk, membranes were incubated with primary antibodies at 4°C overnight and then incubated with HRP-conjugated secondary antibodies for 1 hour at room temperature. Protein signals were visualized using a ChemiDoc Imaging System (Bio-Rad, USA).

RNA isolation and RT-qPCR

Total RNA was extracted using TRIzol regent (Invitrogen, USA). RNA was converted to cDNA using a PrimeScript RT reagent kit (Takara, Japan) and RT-qPCR was performed with SYBR Green Supermix (Takara, Japan). The comparative Ct method (ΔΔCt) was used to analyze the relative expression from RT-qPCR experiments and *GAPDH* was used for normalization. Specific primer pairs were used: *GAPDH* (Homo sapiens), 5'-GGAAGCTTGTCATCAATGGAAATC-3'(Forward), 5'-TGATGACCCTTTTGGCTCCC-3'(Reverse); *BACH1* (Homo sapiens), 5'-GAACAGGGCTACTCGCAAAG-3'(Forward), 5'-AAAGGGCAGTTGACGGAAC-3'(Reverse); *Gapdh* (Mus musculus), 5'-TCAACAGCAACTCCCACTCTTCCA-3' (Forward), 5'- ACCCTGTTGCTGTAGCCGTATTCA-3' (Reverse); *Bach1* (Mus musculus), 5'-CACCTGACCGCCGCTTG-3'(Forward), 5'-TCGTAGGCAAATACCGCACT-3' (Reverse).

Colony formation assay

In colony formation assay, cells (500 cells/well) were seeded in six-well plates and incubated for 2 weeks. Then, the resulting colonies were washed with PBS, fixed with 4% polyoxymethylene, and stained with 0.1% crystal violet. The assay was performed in triplicate for each sample.

EdU-DNA Synthesis Assay

The cell proliferation was evaluated using Cell-Light EdU Apollo567 In Vitro Kit (RiboBio, China). After incubated with 50 μM EdU for 1 h, glioma cells were fixed with 4% paraformaldehyde and incubated with Apollo® reaction mix. The nuclei were stained by Hoechst 33342. Fluorescence was visualized and captured using an inverted microscope (Olympus BX51, Japan).

Transwell assay

5×10^4 cells were seeded into the upper chamber of polycarbonate transwell filters (Millipore, Millicell, USA) containing 200 μL serum-free DMEM. 600 μL of 10% FBS in DMEM was added in lower chambers as a chemotactic agent. Cells were incubated at 37°C for 24 h. The cells on the

lower chamber were fixed with 4% paraformaldehyde and dyed with crystal violet (Beyotime, China). Images were captured by an inverted microscope (Olympus BX51, Japan) and the assay was performed in triplicate for each sample.

Flow cytometry of apoptosis

Flow cytometry of apoptosis was conducted by dual staining using Annexin V-FITC and propidium iodide (PI) (Thermo Fisher Scientific, USA). Cells were collected, resuspended in 1× binding solution, and stained with Annexin V-FITC and PI. The apoptotic cells were analyzed using a flow cytometry (CytoFLEX, Beckman Coulter, USA) and analyzed by a FlowJo software (version 7.6.1).

***In vivo* experiments**

Four-week-old male BALB/c nude mice from Vital River Laboratory Animal Technology (Beijing, China) were used for the construction of GBM xenograft model. U251-shNC and U251-shBACH1 cells were intracranially injected into the brain (1 mm anterior and 2 mm lateral to bregma at a depth of 3mm) of BALB/c nude mice via stereotactic system (51725, Stoelting, USA). 14 days after tumor injection, ulixertinib (80 mg/kg) was applied orally twice daily (every 12 h) for five consecutive days. Tumor-bearing mice were sacrificed when they showed severe neurological symptoms and the brains were fixed with 4% paraformaldehyde for immunohistochemical and HE staining.

Four-week-old male C57BL/6 mice from Vital River Laboratory Animal Technology (Beijing, China) were used for the construction of GL261 murine glioma models. GL261 cells labelled with luciferase were intracranially injected into the brain (1 mm anterior and 2 mm lateral to bregma at a depth of 3mm) of C57BL/6 mice. 12 days after tumor injection, ulixertinib (80 mg/kg) was applied orally twice daily (every 12 h) for five consecutive days and hemin was intraperitoneally injected (50 mg/kg) daily (every 24 h) for five consecutive days. For the construction of another GL261 murine glioma model, GL261-shNC-Luc and GL261-shBach1-Luc cells were intracranially injected. Starting from day 12, ulixertinib (80 mg/kg) was applied orally twice daily (every 12 h) for five consecutive days. All tumor-bearing mice were captured by IVIS 10 days (day 10), 21days (day 21), and 28 days (day 28) after tumor injection and sacrificed when they showed severe neurological symptoms.

Animal experiments in this research were approved by the institutional animal care and use committee of Renmin Hospital of Wuhan University.

***In vivo* imaging**

In vivo Imaging System (IVIS) was applied for the visualization of GL261-luc in C57BL/6 mice. 10 mg D-Luciferin potassium was injected (ST196, Beyotime) for visualization in each mouse and the tumor was captured using an IVIS (PerkinElmer IVIS Lumina, USA).

Immunohistochemical staining

Tumor tissues of animal models were embedded with paraffin and sectioned. The sections were deparaffinized, hydrated, and antigen repaired with 10mM sodium citrate (pH, 6.0). The samples were incubated in 3% H_2O_2 to remove endogenous peroxidase and blocked by 1% Albumin Bovine V (Beyotime, China). Then, the slides were incubated with primary antibody overnight at 4°C and

visualized by a 3,3′-diaminobenzidine (DAB) kit (Solarbio, China). The images were captured under an inverted microscope (Olympus BX51, Japan)

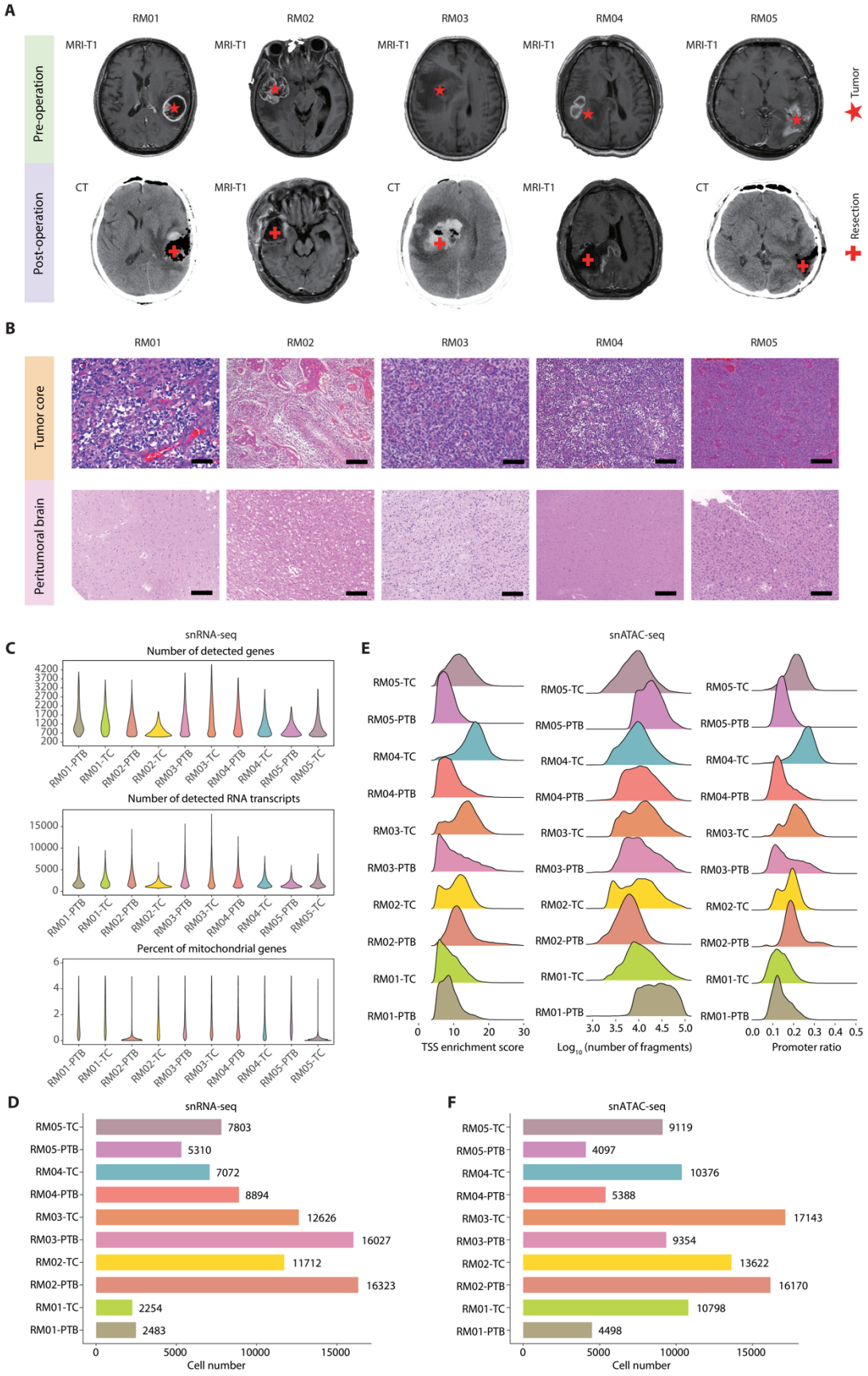
A
RM01
RM02
RM03
RM04
RM05
Pre-operation
Post-operation
MRI-T1
CT
Tumor
Resection
B
Tumor core
Peritumoral brain
C
snRNA-seq
Number of detected genes
Number of detected RNA transcripts
Percent of mitochondrial genes
RM01-PTB
RM01-TC
RM02-PTB
RM02-TC
RM03-PTB
RM03-TC
RM04-PTB
RM04-TC
RM05-PTB
RM05-TC
D
snRNA-seq
7803
5310
7072
8894
12626
16027
11712
16323
2254
2483
Cell number
E
snATAC-seq
TSS enrichment score
Log10 (number of fragments)
Promoter ratio
F
snATAC-seq
9119
4097
10376
5388
17143
9354
13622
16170
10798
4498
Cell number

Fig. S1. Sample profile and quality control of single-cell data. (**A**) Pre-operation and post-operation brain imaging. Asterisks mark the original tumor site. Pluses mark the resection site. (**B**) Representative HE staining on each sample. Scale bars: 100 μm. (**C**) Violin diagrams showing the quality for snRNA-seq. The gene number, RNA count, and mitochondrial gene ratio per cell after quality control are shown. (**D**) Bar plot of cell number after quality control in snRNA-seq. (**E**) Ridge diagrams showing the quality for snATAC-seq. The TSS enrichment score, $\log_{10}$(unique nuclear fragments), and promoter ratio per cell after quality control are shown. (**F**) Bar plot of cell number after quality control in snATAC-seq.

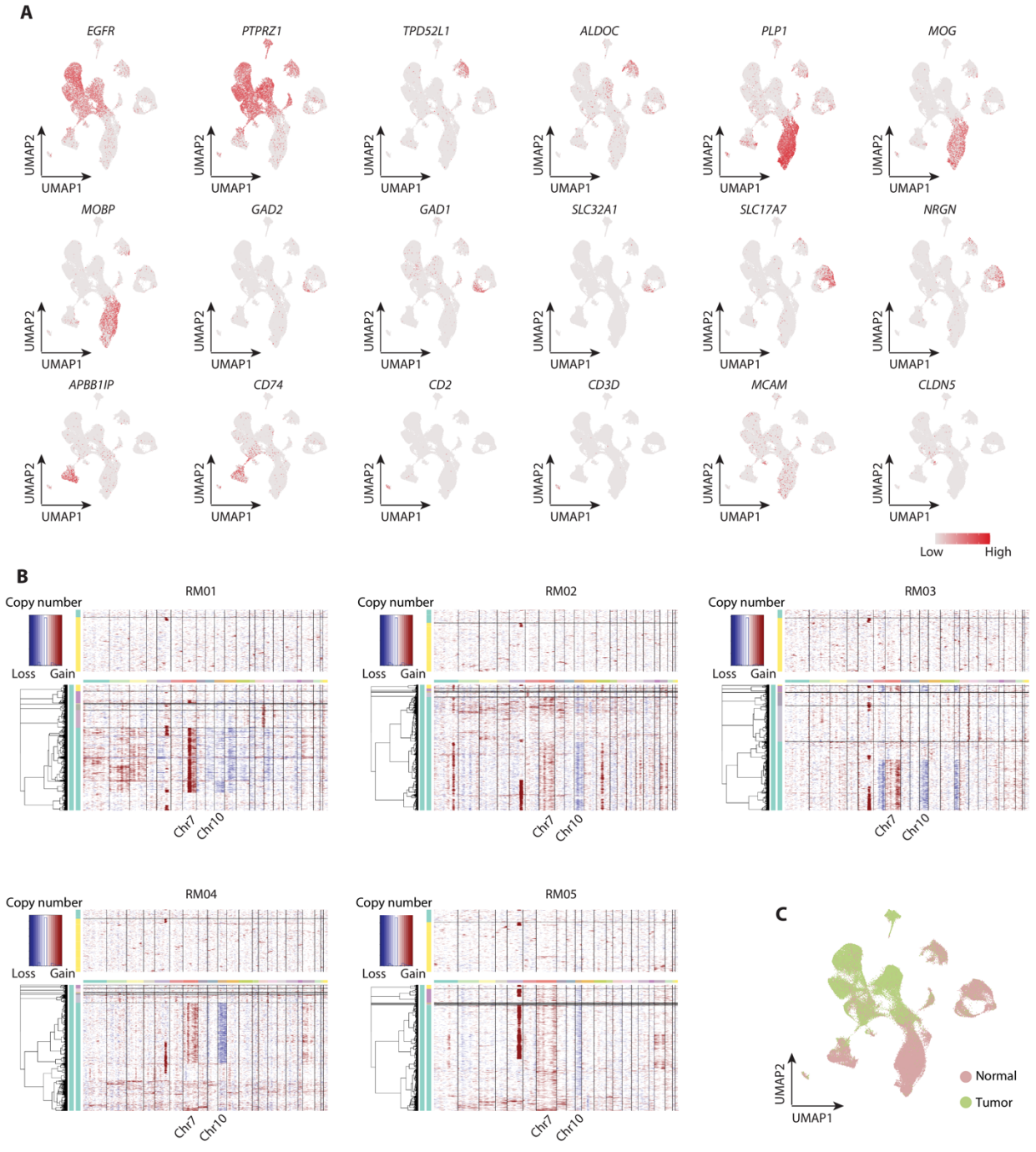

Fig. S2. Basis for cell type identification in snRNA-seq. (**A**) UMAP showing the expression of canonical marker genes for cell type identification. The redder the color, the higher the expression. (**B**) CNV analysis of putative malignant cells with InferCNV. The upper part of each heatmap represents normal cells and are considered as reference cells, containing myeloid cells and oligodendrocytes from the peritumoral brain of each patient. The lower part represents observation cells. (**C**) UMAP colored by malignant status (tumor or normal) inferred by inferCNV.

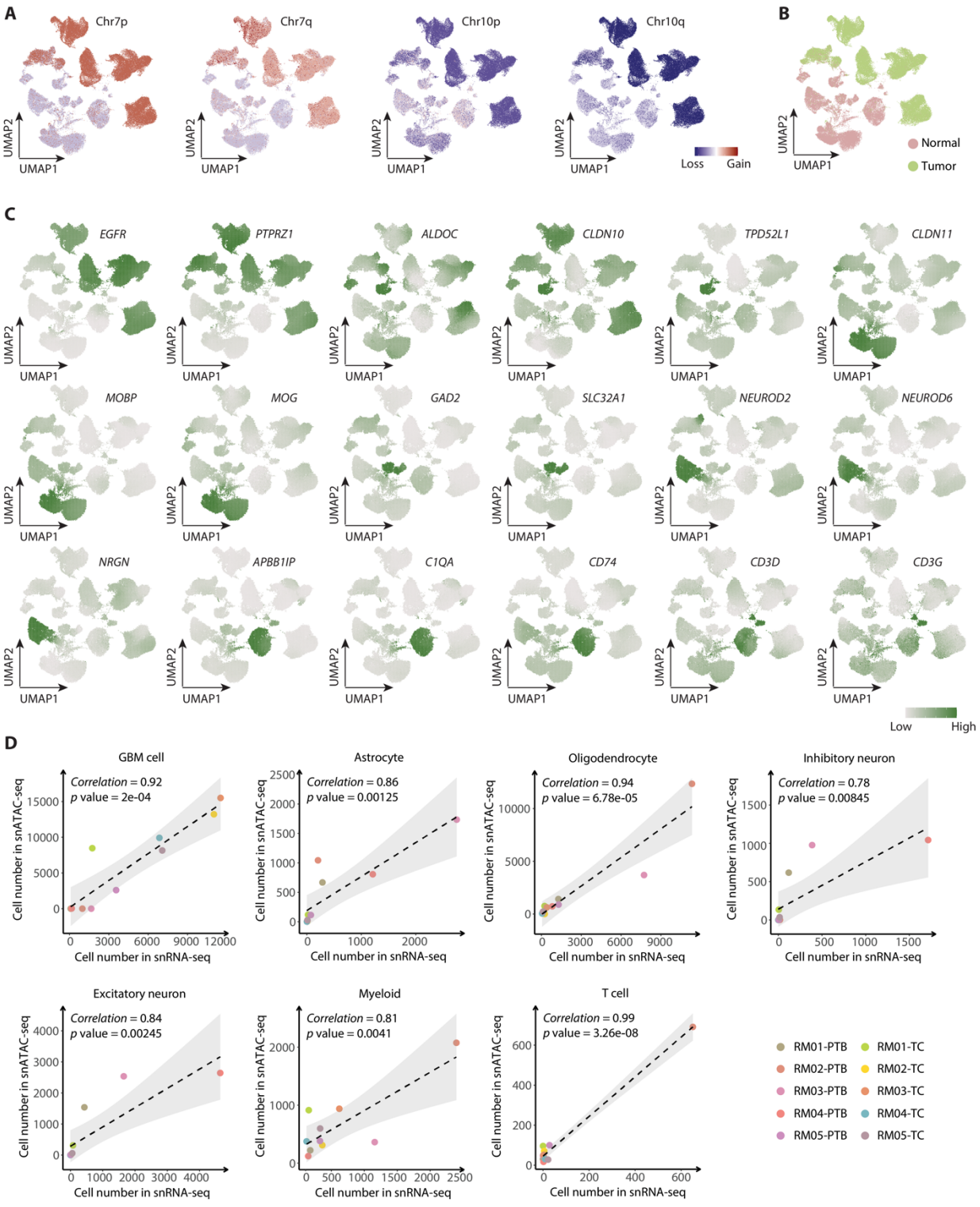

Fig. S3. Basis for cell type identification in snATAC-seq. (**A**) UMAP colored by canonical CNVs of GBM cells, including chr7p (+), chr7q (+), chr10p (-), and chr10q (-). (**B**) UMAP colored by malignant status (tumor or normal) inferred by Copy-scAT. (**C**) UMAP of gene activity score of canonical marker genes for cell type identification. (**D**) Scatter plots showing

the correlation of captured numbers of each cell type between snRNA-seq and snATAC-seq. Dots are colored by cell types.

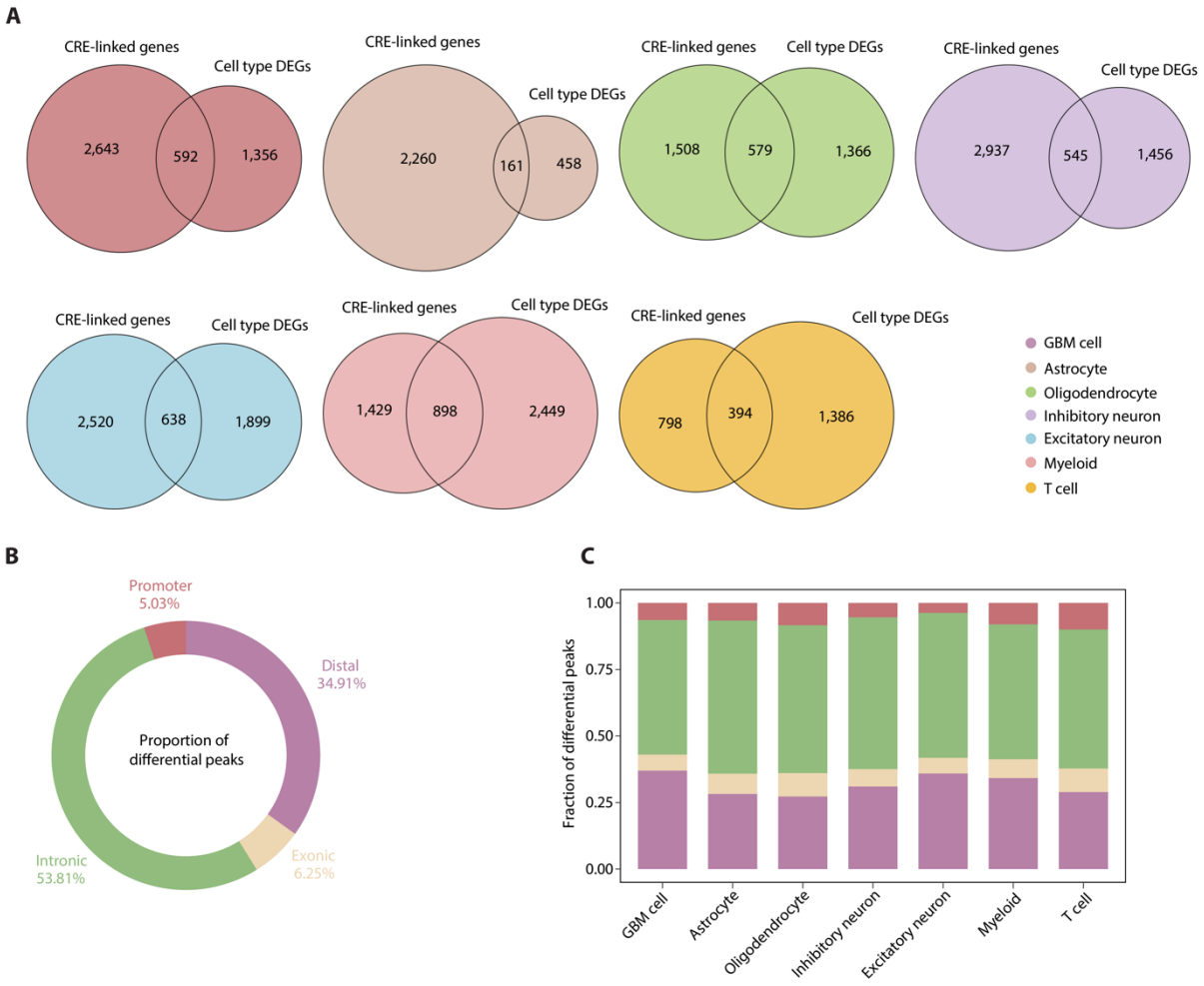

Fig. S4. Gene-linked CREs showing cell type specificity. (**A**) Venn diagrams for each cell type denoting the overlaps between the CRE-linked genes and upregulated genes in that cell type (cell type DEGs). (**B**) Donut diagram showing the genomic distribution of all differential peaks. (**C**) Stacked bar chart showing the genomic distribution of differential peaks across different cell types.

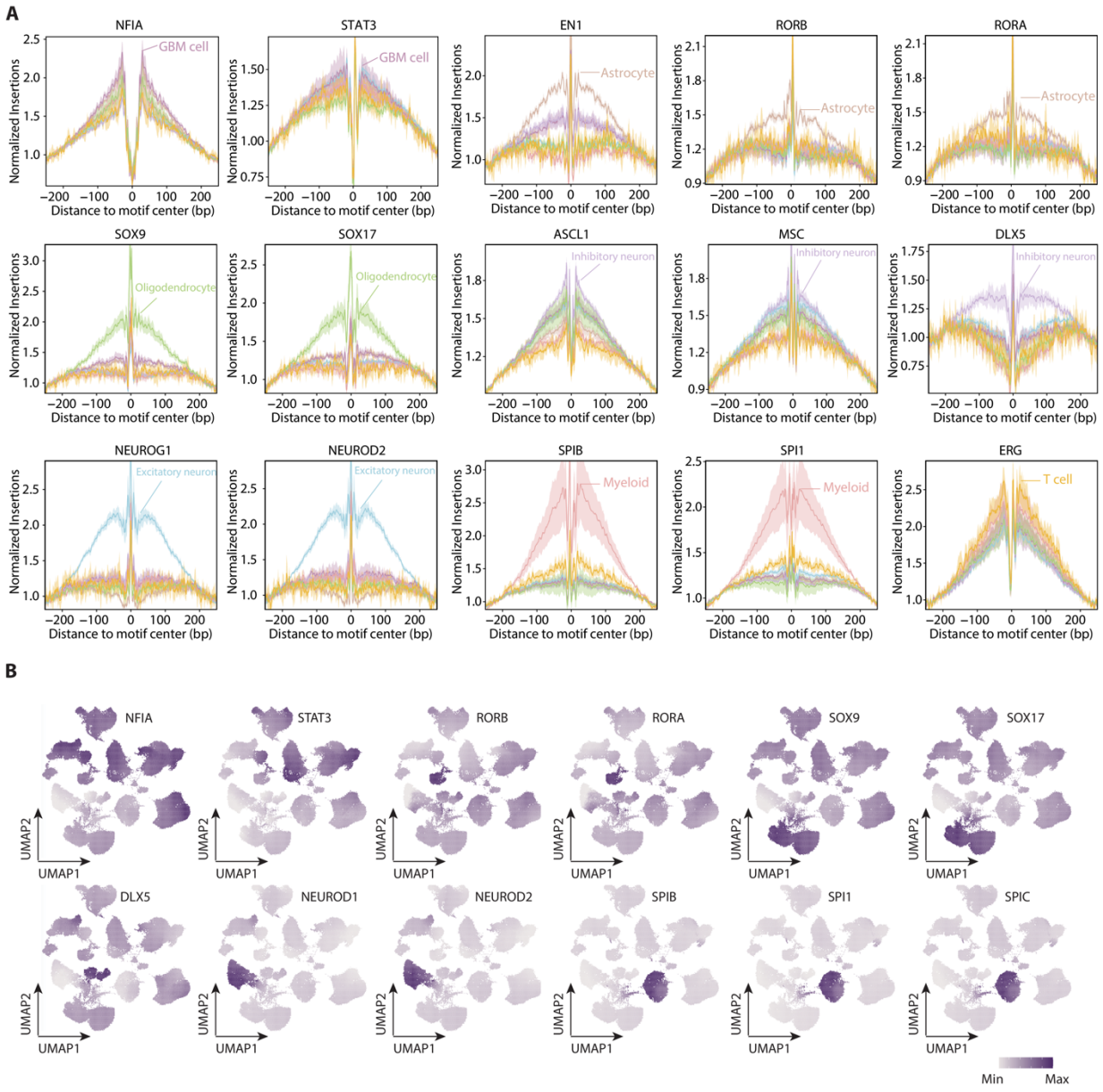

Fig. S5. TF regulation for each cell type. (**A**) Tn5 bias-adjusted TF footprints for cell-type specific regulators in snATAC-seq. (**B**) UMAP showing the cell type specific motif variability from snATAC-seq.

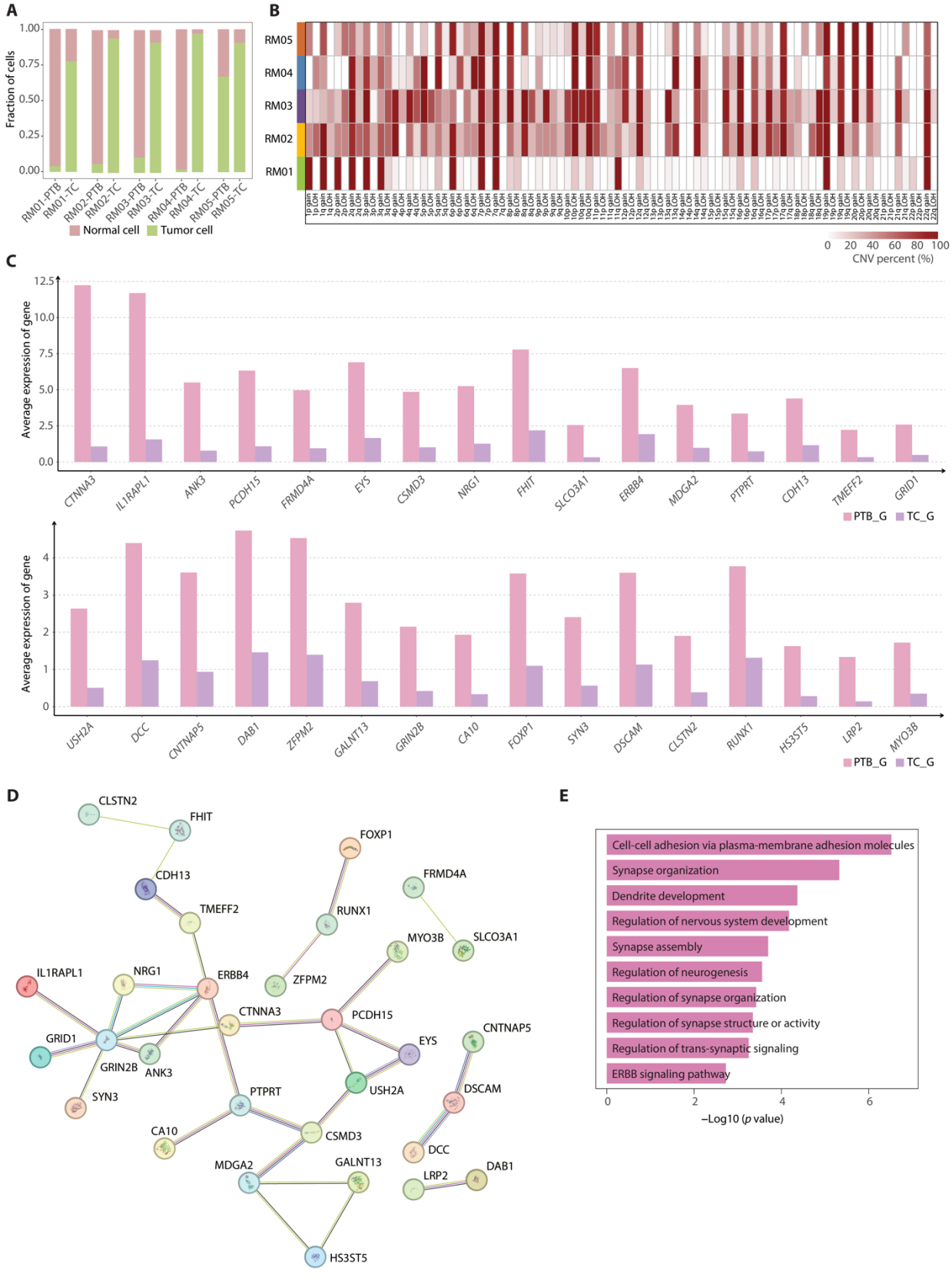
A
Fraction of cells
1.00
0.75
0.50
0.25
0.00
RM01-PTB
RM01-TC
RM02-PTB
RM02-TC
RM03-PTB
RM03-TC
RM04-PTB
RM04-TC
RM05-PTB
RM05-TC
Normal cell
Tumor cell
B
RM05
RM04
RM03
RM02
RM01
0
20
40
60
80
100
CNV percent (%)
C
Average expression of gene
CTNNA3
IL1RAPL1
ANK3
PCDH15
FRMD4A
EYS
CSMD3
NRG1
FHIT
SLCO3A1
ERBB4
MDGA2
PTPRT
CDH13
TMEFF2
GRID1
PTB_G
TC_G
USH2A
DCC
CNTNAP5
DAB1
ZFPM2
GALNT13
GRIN2B
CA10
FOXP1
SYN3
DSCAM
CLSTN2
RUNX1
HS3ST5
LRP2
MYO3B
D
CLSTN2
FHIT
FOXP1
CDH13
FRMD4A
TMEFF2
RUNX1
MYO3B
SLCO3A1
IL1RAPL1
NRG1
ERBB4
ZFPM2
CTNNA3
PCDH15
CNTNAP5
GRID1
EYS
GRIN2B
ANK3
USH2A
DSCAM
SYN3
PTPRT
CA10
CSMD3
DCC
MDGA2
GALNT13
DAB1
LRP2
HS3ST5
E
Cell-cell adhesion via plasma-membrane adhesion molecules
Synapse organization
Dendrite development
Regulation of nervous system development
Synapse assembly
Regulation of neurogenesis
Regulation of synapse organization
Regulation of synapse structure or activity
Regulation of trans-synaptic signaling
ERBB signaling pathway
0
2
4
6
–Log10 (p value)

Fig. S6. GBM cells from the two regions harboring distinct transcription characteristics. (**A**) Bar plot showing the percentage of GBM cells and non-GBM cells in each sample. (**B**) The summary CNV profiles of GBM cells for each patient. The CNV levels were categorized by the chromosome arm and labeled as gain or loss. Color in the heatmap represents the proportion of cells harboring the CNV events in each individual patient. (**C**) Bar plots showing the expression of PTB_G signature genes in PTB_G and TC_G. (**D**) Network showing the PPI in PTB_G signature identified by STRING (*53*). (**E**) Bar plot showing the enriched GO terms of PTB_G signature genes.

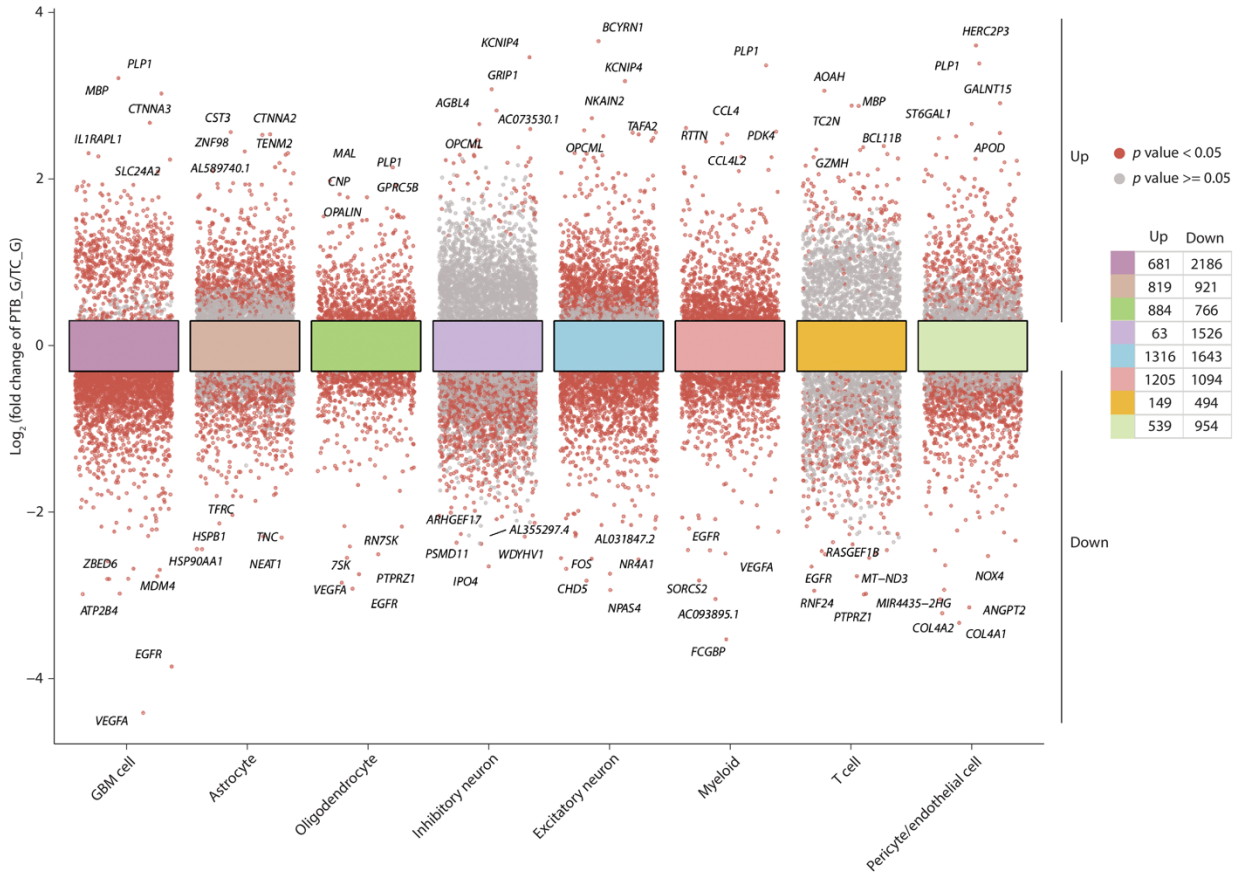

Fig. S7. The altered microenvironment across the two regions. Scatter plot showing the DEGs across the cell types.

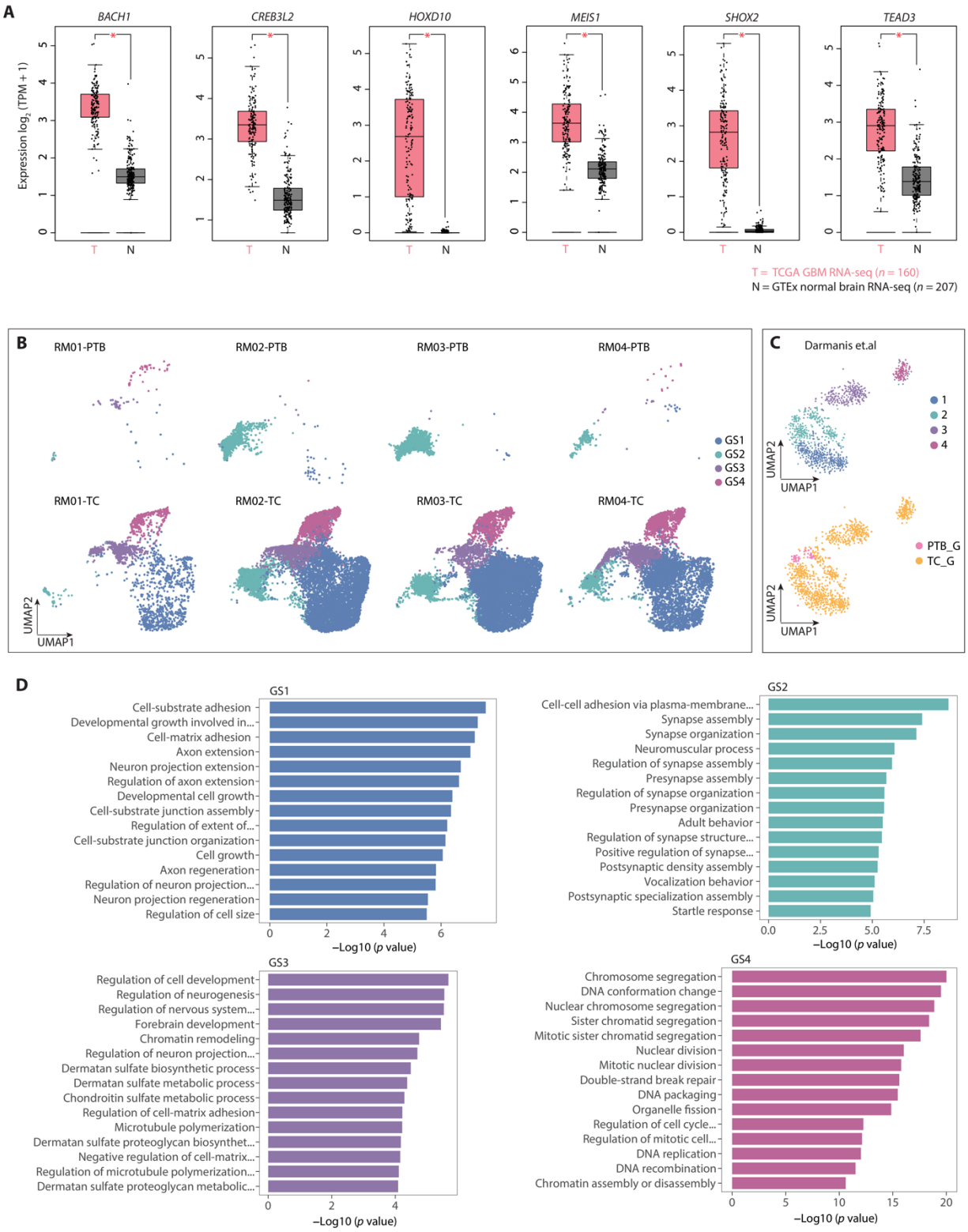

Fig. S8. Subclustering for GBM cells. (**A**) Boxplots showing the expression of the identified TFs in normal brain and GBM. (**B**) UMAP of GBM cells subclusters (i.e., GS1, GS2, GS3, and GS4) split by samples. The top panel represents samples from PTB, and the bottom panel

represents samples from the TC. The plot is colored by subclusters. (**C**) UMAP showing GBM cell populations from Darmanis et.al. (**D**) Bar plot of GO terms (biological process) enriched in each subcluster of GBM cells from Fig. 5C.

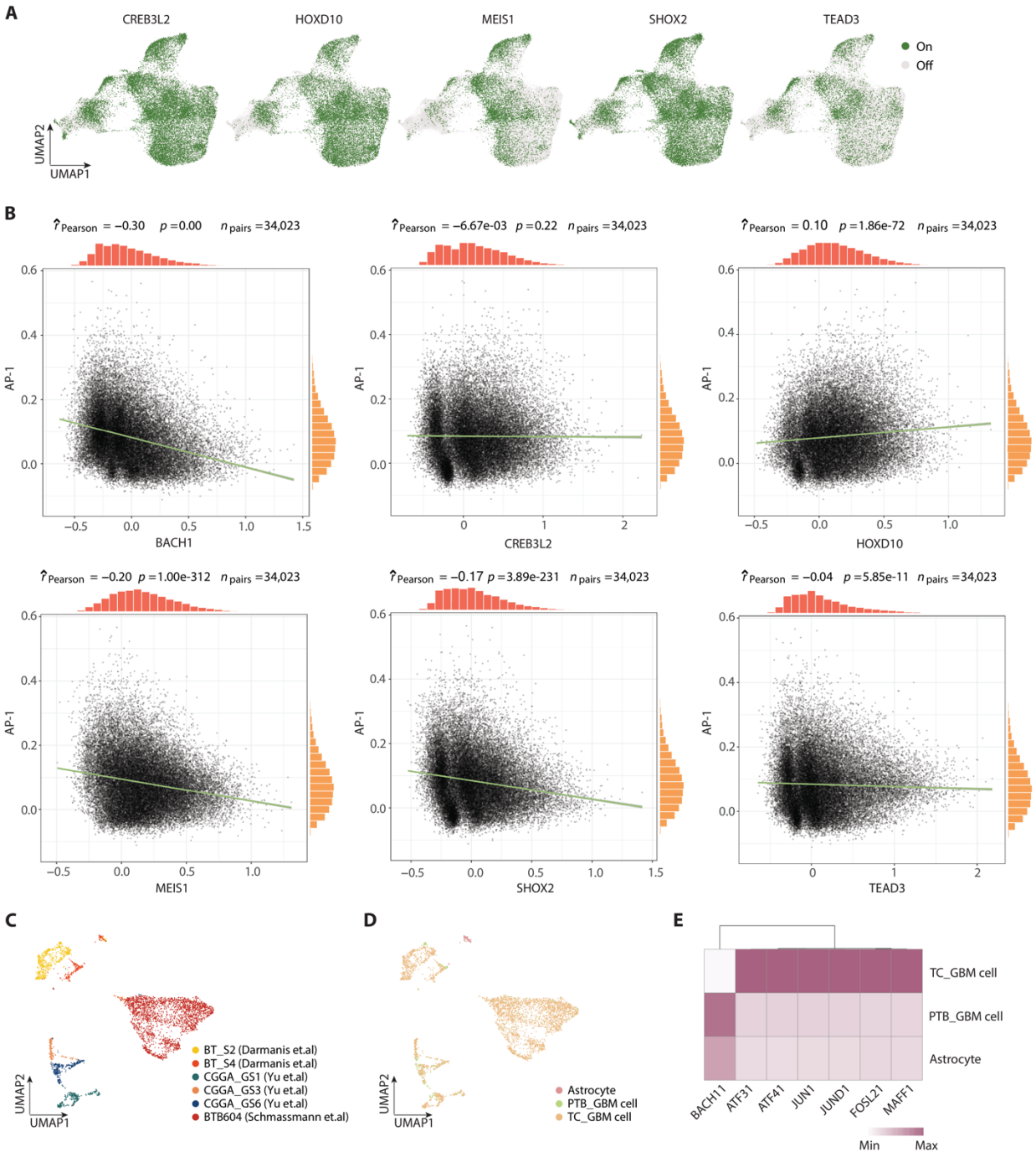

Fig. S9. The correlation analysis of candidate TFs with AP-1. (**A**) UMAP diagrams showing the activation of candidate regulons in GBM cells. (**B**) Scatter plots showing the expression correlation of the six candidate regulons with AP-1 regulons. (**C** and **D**) UMAP plots of cells collected from public datasets, colored by sample origins (C) and cell populations (D), respectively. (**E**) Heatmap showing the activity of BACH1 and AP-1 in three groups.

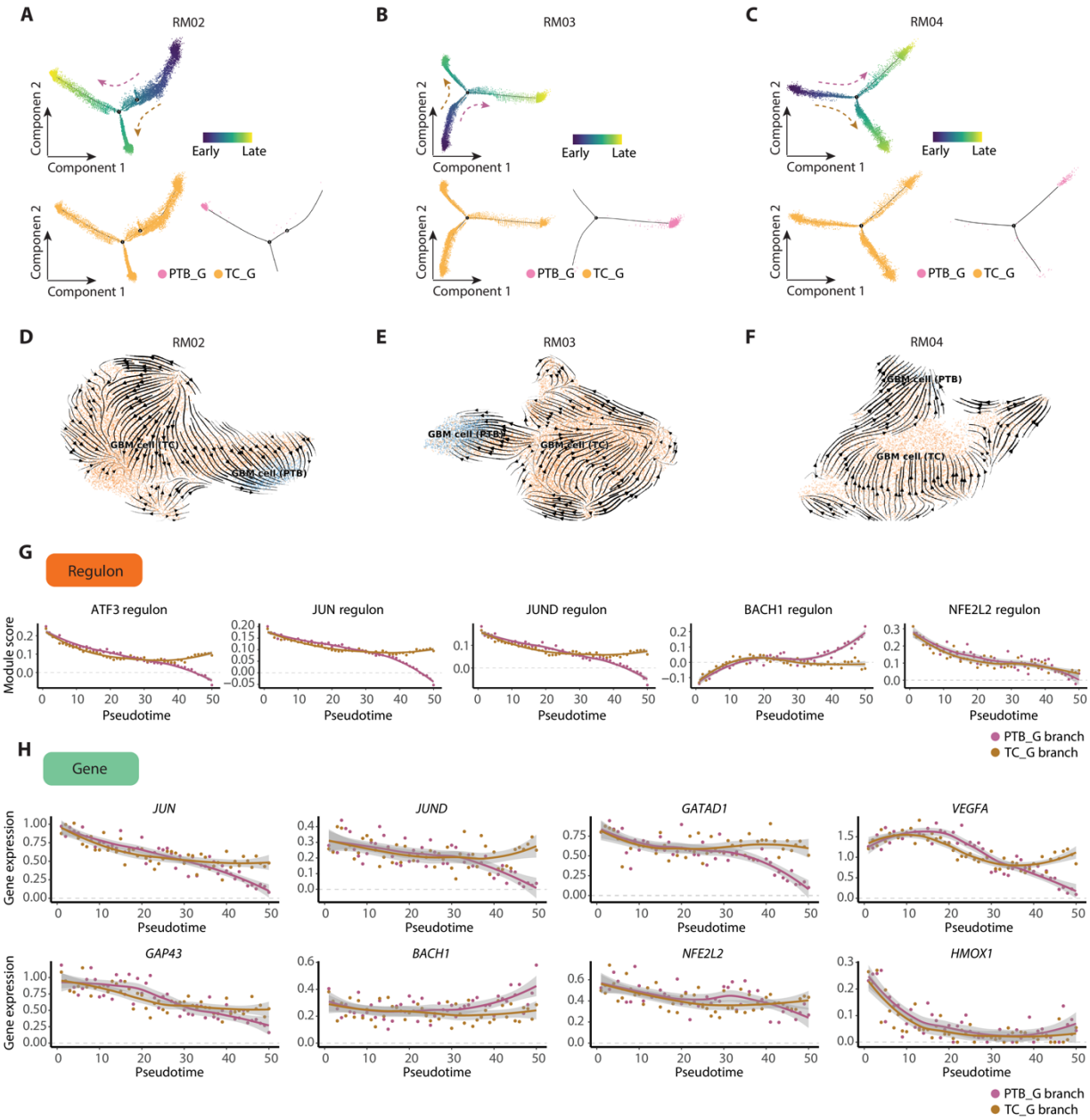

Fig. S10. Pseudo-time trajectory for GBM cells. (**A-C**) Monocle trajectory for GBM cells from the two regions in RM02 (A), RM03 (B), and RM04 (C). The top image indicates the differentiation time. The bottom two images show the location for different regions of GBM cells. (**D-F**) RNA velocities for GBM cells in RM02 (D), RM03 (E), and RM04 (F). The associated streamlines are represented in the plots and dots are colored by regions of GBM cells. (**G** and **H**) Scatter plots for scores of selected regulons (G) and expression of genes (H). The colors represent different branches.

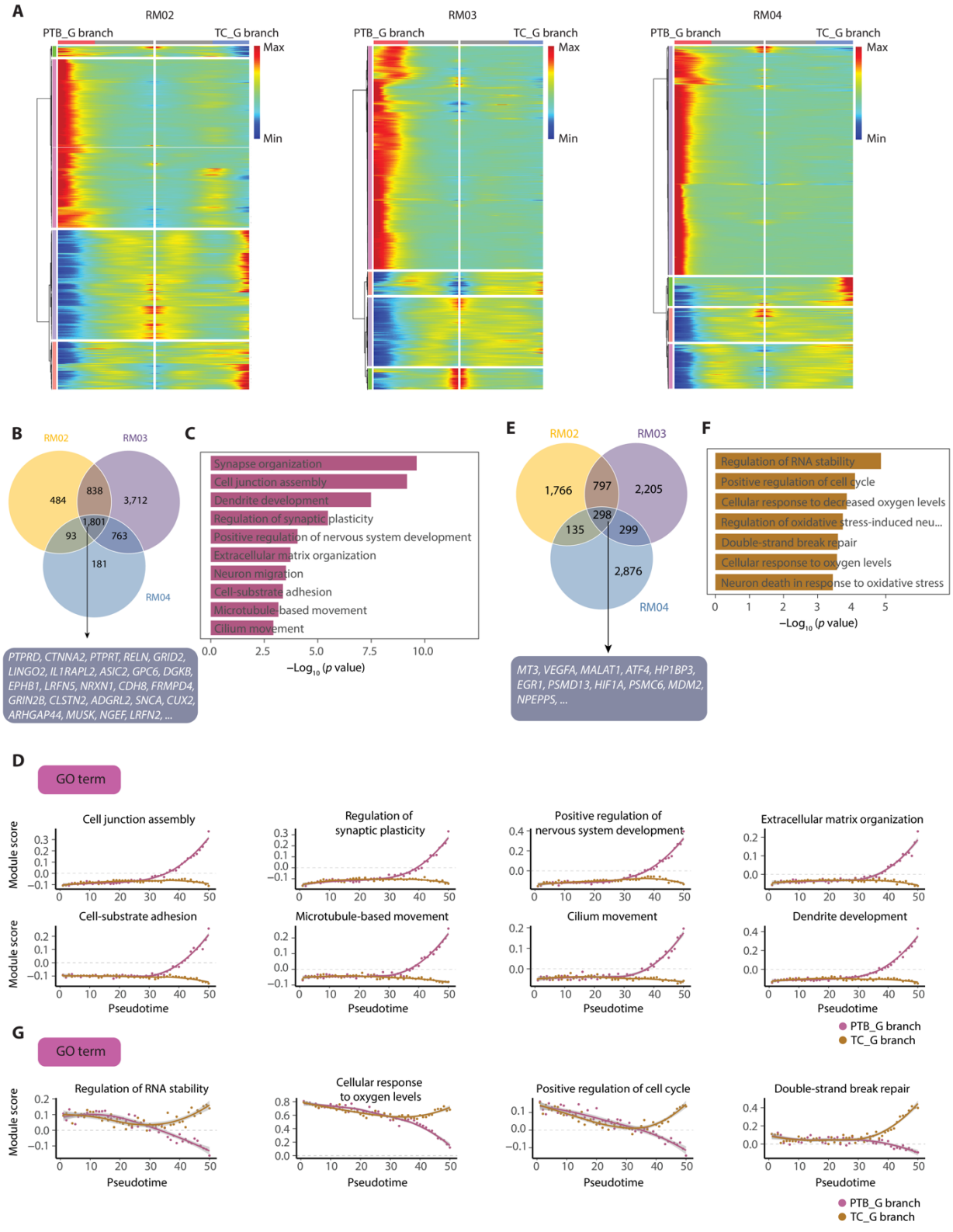

Fig. S11. Changes of different characteristics along the monocle trajectory. (**A**) Heatmap showing the kinetic clusters of branch-dependent genes for RM02 (left), RM03 (mid), and RM04

(right). (**B**) Venn diagram showing the intersection of genes from three patients, with their expression increasing along the branch located by GBM cells from tumor core. (**C)** Bar plot of GO terms (biological process) enriched by intersection genes for fig. S11B. (**D**) Scatter plots of module scores for GO terms from fig. S11C. (**E**) Venn diagram showing the intersection of genes from three patients, with their expression increasing along the branch located by GBM cells from tumor core. (**F**) Bar plot of GO terms (biological process) enriched by intersection genes for fig. S11E. (**G**) Scatter plots of module scores for GO terms from fig. S11F.

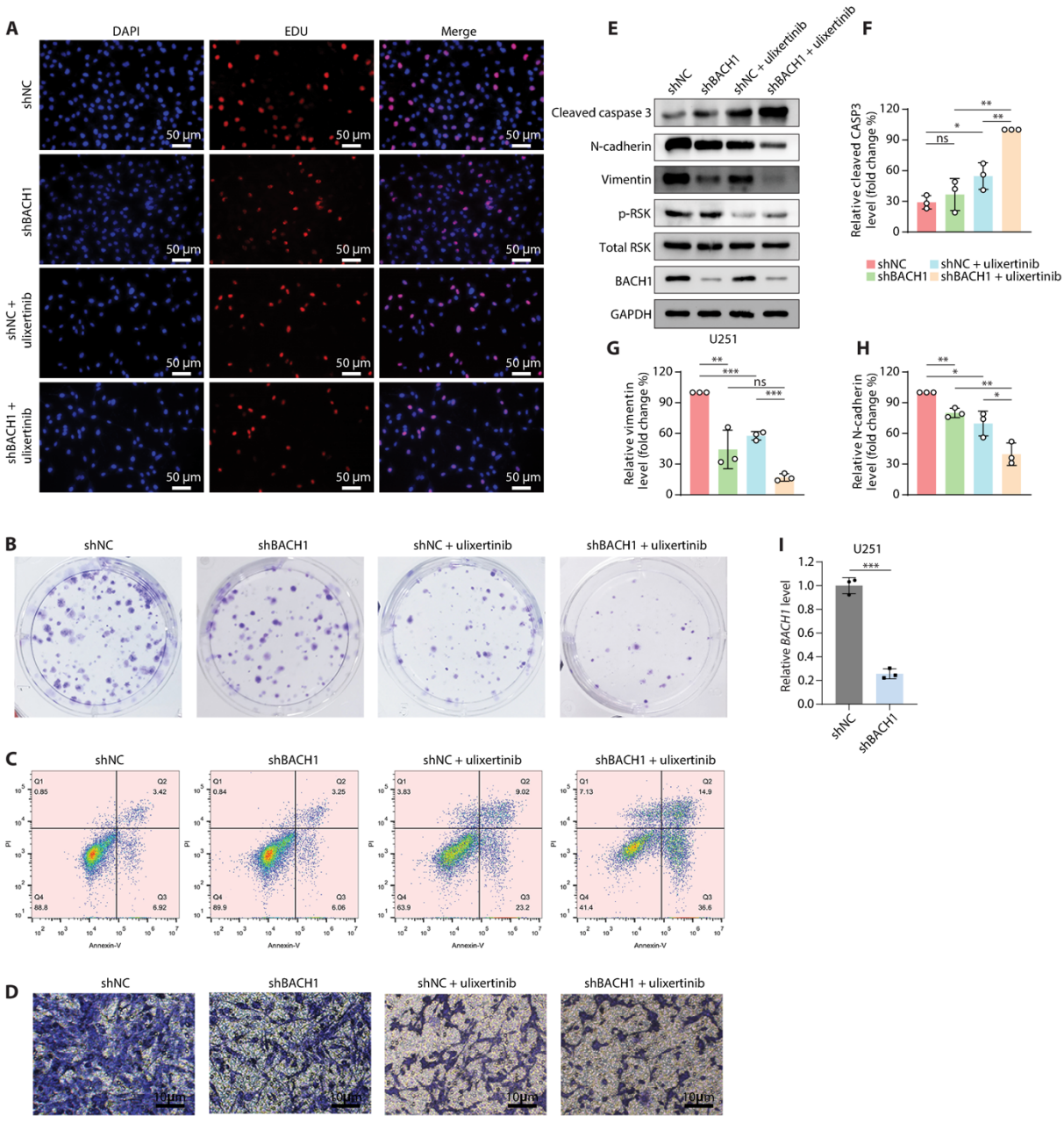

Fig. S12. Combination therapy in GBM suppression. (**A-D**) Representative images showing BrdU incorporation (A), colony-formation (B), flow cytometry (C), and transwell migration (D) assays of the indicated groups in Fig. 6A. (**E-H**) Western blot (E) of indicated proteins in U251 cells with multiple treatments, and the quantification were shown (F-H) (n = 3 biological replicates). (**I**) qRT-PCR of BACH1 mRNA expression in U251 cells with or without BACH1 depletion. n = 3 technical replicates. *$p < 0.05$, **$p < 0.01$, and ***$p < 0.001$.

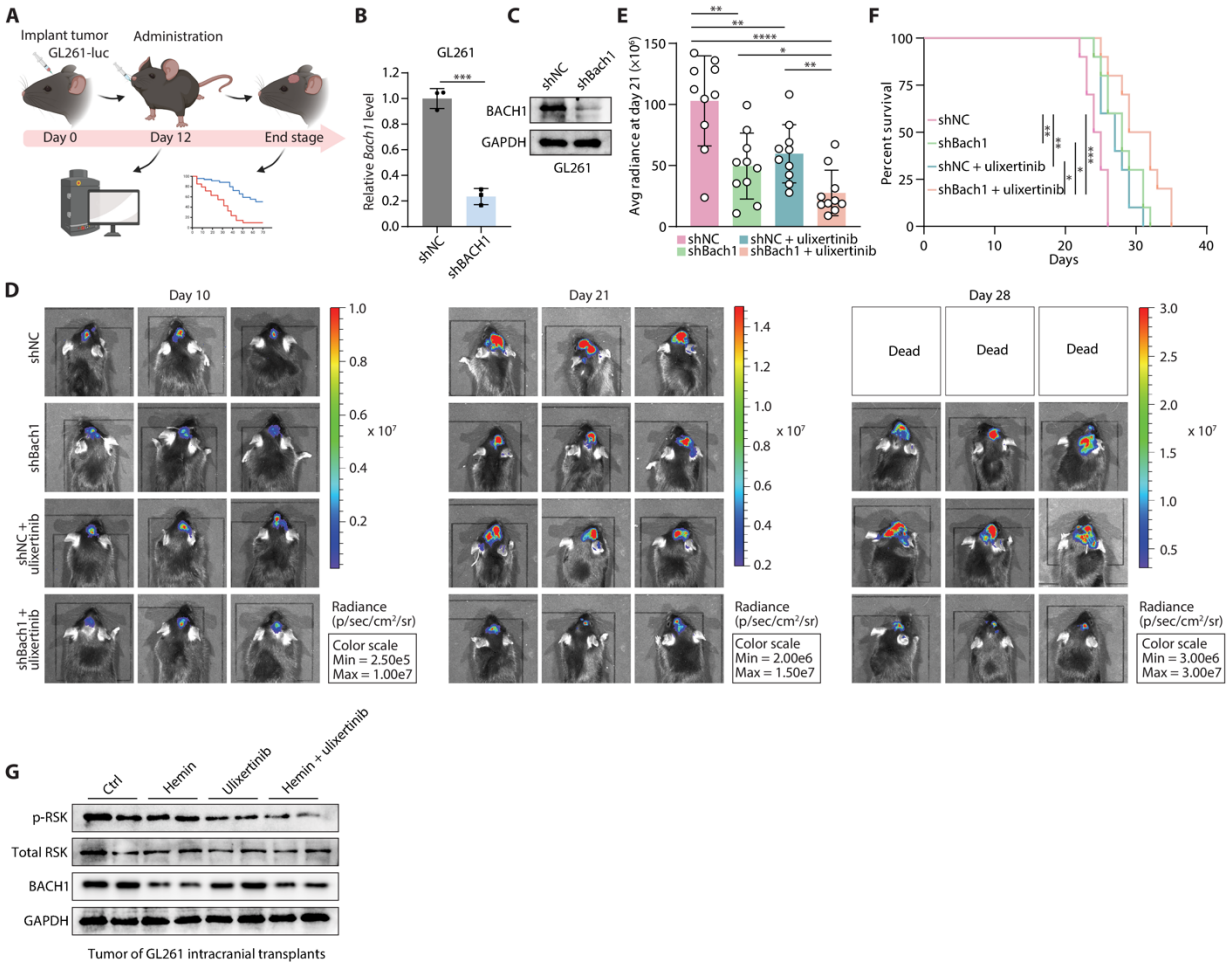

Fig. S13. Combination therapy suppresses tumor growth and improves survival in GL261-derived mouse models. (**A**) Illustration depicting the therapy schedule. Luciferase-expressing GL261 cells (with or without BACH1 depletion) were intracranially injected into nude mice on day 0. Treatment started on day 12, with or without ulixertinib (80 mg/kg) orally twice daily (every 12 h) for 5 days. (n = 10 for each group). (**B**) qRT-PCR of BACH1 mRNA expression in GL261 cells with or without BACH1 depletion. n = 3 technical replicates. (**C**) Western blot showing the BACH1 protein in GL261 cells with or without BACH1 depletion. (**D**) Luminescence intensity showing tumors in representative mice over time. (**E**) Quantitative radiance in the experimental group on day 21. (**F**) The survival time of the indicated groups of mice in (A). (**G**) Western blot showing the indicated proteins in mouse tumor lysates from Fig. 6F. *$p < 0.05$, **$p < 0.01$, ***$p < 0.001$, and ****$p < 0.0001$.

Table S1. Clinical and experimental information for surgical samples.

Table S2. The summary statistics for snRNA-seq data.

Table S3. The summary statistics for snATAC-seq data.

Table S4. List of DEGs in cell types from snRNA-seq.

Table S5. The compositions of cell types in snRNA-seq and snATAC-seq.

Table S6. ChIP-seq datasets employed in genome track visualization.

Table S7. Distribution of CNVs on the chromosome arms for patients in snRNA-seq.

Table S8. Pan cancer signatures for feature scoring in GBM cells.

Table S9. List of DEGs between GBM cells from two regions and astrocyte from peritumoral brain.

Table S10. List of DEGs of GBM cells between two regions.

Table S11. The percentages of composition for the four GBM cellular states.

Table S12. Lists of motifs enriched in four GBM cellular states in snATAC-seq.

Table S13. List of potential regulons for PTB_G.

Table S14. GO terms (biological processes) enriched in GBM cell subclusters.

Table S15. The fractions of GBM cells with activated regulon for AP1 or/and other candidates.

Table S16. The numbers of cells activated for AP1 or/and BACH1 regulons.

Table S17. Lists of genes with elevated expression along the two monocle branches separately across the three patients.

REFERENCES AND NOTES

1. Q. T. Ostrom, M. Price, C. Neff, G. Cioffi, K. A. Waite, C. Kruchko, J. S. Barnholtz-Sloan, N. Nagarajan, B. B. Cordeiro, N. Willmarth, M. Penas-Prado, M. R. Gilbert, CBTRUS statistical report: Primary brain and other central nervous system tumors diagnosed in the United States in 2016-2020. *Neuro Oncol.* **26**, iii1–iii53 (2024).

2. R. Stupp, W. P. Mason, M. J. Van Den Bent, M. Weller, B. Fisher, M. J. B. Taphoorn, K. Belanger, A. A. Brandes, C. Marosi, U. Bogdahn, J. Curschmann, R. C. Janzer, S. K. Ludwin, T. Gorlia, A. Allgeier, D. Lacombe, J. G. Cairncross, E. Eisenhauer, R. O. Mirimanoff; European Organisation for Research and Treatment of Cancer Brain Tumor and Radiotherapy Groups; National Cancer Institute of Canada Clinical Trials Group, Radiotherapy plus concomitant and adjuvant temozolomide for glioblastoma. *N. Engl. J. Med.* **352**, 987–996 (2005).

3. T. S. van Solinge, L. Nieland, E. A. Chiocca, M. L. D. Broekman, Advances in local therapy for glioblastoma - taking the fight to the tumour. *Nat. Rev. Neurol.* **18**, 221–236 (2022).

4. M. T. Milano, P. Okunieff, R. S. Donatello, N. A. Mohile, J. Sul, K. A. Walter, D. N. Korones, Patterns and timing of recurrence after temozolomide-based chemoradiation for glioblastoma. *Int. J. Radiat. Oncol. Biol. Phys.* **78**, 1147–1155 (2010).

5. K. Kallenberg, T. Goldmann, J. Menke, H. Strik, H. C. Bock, F. Stockhammer, J. H. Buhk, J. Frahm, P. Dechent, M. Knauth, Glioma infiltration of the corpus callosum: early signs detected by DTI. *J. Neurooncol.* **112**, 217–222 (2013).

6. M. D. Prados, S. A. Byron, N. L. Tran, J. J. Phillips, A. M. Molinaro, K. L. Ligon, P. Y. Wen, J. G. Kuhn, I. K. Mellinghoff, J. F. de Groot, H. Colman, T. F. Cloughesy, S. M. Chang, T. C. Ryken, W. D. Tembe, J. A. Kiefer, M. E. Berens, D. W. Craig, J. D. Carpten, J. M. Trent, Toward precision medicine in glioblastoma: The promise and the challenges. *Neuro Oncol.* **17**, 1051–1063 (2015).

7. K. Petrecca, M. C. Guiot, V. Panet-Raymond, L. Souhami, Failure pattern following complete resection plus radiotherapy and temozolomide is at the resection margin in patients with glioblastoma. *J Neurooncol.* **111**, 19–23 (2013).

8. D. Odde, Glioblastoma cell invasion: Go? Grow? Yes. *Neuro Oncol.* **25**, 2163–2164 (2023).

9. T. J. Brown, M. C. Brennan, M. Li, E. W. Church, N. J. Brandmeir, K. L. Rakszawski, A. S. Patel, E. B. Rizk, D. Suki, R. Sawaya, M. Glantz, Association of the extent of resection with survival in glioblastoma: A systematic review and meta-analysis. *JAMA Oncol.* **2**, 1460–1469 (2016).

10. S. Darmanis, S. A. Sloan, D. Croote, M. Mignardi, S. Chernikova, P. Samghababi, Y. Zhang, N. Neff, M. Kowarsky, C. Caneda, G. Li, S. D. Chang, I. D. Connolly, Y. Li, B. A. Barres, M. H. Gephart, S. R. Quake, Single-cell RNA-seq analysis of infiltrating neoplastic cells at the migrating front of human glioblastoma. *Cell Rep* **21**, 1399–1410 (2017).

11. T. Shekarian, C. P. Zinner, E. M. Bartoszek, W. Duchemin, A. T. Wachnowicz, S. Hogan, M. M. Etter, J. Flammer, C. Paganetti, T. A. Martins, P. Schmassmann, S. Zanganeh, F. Le Goff, M. G. Muraro, M. F. Ritz, D. Phillips, S. S. Bhate, G. L. Barlow, G. P. Nolan, C. M. Schürch, G. Hutter, Immunotherapy of glioblastoma explants induces interferon-γ responses and spatial immune cell rearrangements in tumor center, but not periphery. *Sci. Adv.* **8**, eabn9440 (2022).

12. G. Andrieux, T. Das, M. Griffin, J. Straehle, S. M. L. Paine, J. Beck, M. Boerries, D. H. Heiland, S. J. Smith, R. Rahman, S. Chakraborty, Spatially resolved transcriptomic profiles reveal unique defining molecular features of infiltrative 5ALA-metabolizing cells associated with glioblastoma recurrence. *Genome Med.* **15**, 48 (2023).

13. J. H. Lee, J. E. Lee, J. Y. Kahng, S. H. Kim, J. S. Park, S. J. Yoon, J. Y. Um, W. K. Kim, J. K. Lee, J. Park, E. H. Kim, J. H. Lee, J. H. Lee, W. S. Chung, Y. S. Ju, S. H. Park, J. H. Chang, S. G. Kang, J. H. Lee, Human glioblastoma arises from subventricular zone cells with low-level driver mutations. *Nature* **560**, 243–247 (2018).

14. I. Spiteri, G. Caravagna, G. D. Cresswell, A. Vatsiou, D. Nichol, A. Acar, L. Ermini, K. Chkhaidze, B. Werner, R. Mair, E. Brognaro, R. G. W. Verhaak, G. Sanguinetti, S. G. M. Piccirillo, C. Watts, A. Sottoriva, Evolutionary dynamics of residual disease in human glioblastoma. *Ann. Oncol.* **30**, 456–463 (2019).

15. K. Soureas, M. A. Papadimitriou, K. Panoutsopoulou, K. M. Pilala, A. Scorilas, M. Avgeris, Cancer quiescence: Non-coding RNAs in the spotlight. *Trends Mol. Med.* **29**, 843–858 (2023).

16. F. Antonica, L. Santomaso, D. Pernici, L. Petrucci, G. Aiello, A. Cutarelli, L. Conti, A. Romanel, E. Miele, T. Tebaldi, L. Tiberi, A slow-cycling/quiescent cells subpopulation is involved in glioma invasiveness. *Nat Commun.* **13**, 4767 (2022).

17. F. P. Barthel, K. C. Johnson, F. S. Varn, A. D. Moskalik, G. Tanner, E. Kocakavuk, K. J. Anderson, O. Abiola, K. Aldape, K. D. Alfaro, D. Alpar, S. B. Amin, D. M. Ashley, P. Bandopadhayay, J. S. Barnholtz-Sloan, R. Beroukhim, C. Bock, P. K. Brastianos, D. J. Brat, A. R. Brodbelt, A. F. Bruns, K. R. Bulsara, A. Chakrabarty, A. Chakravarti, J. H. Chuang, E. B. Claus, E. J. Cochran, J. Connelly, J. F. Costello, G. Finocchiaro, M. N. Fletcher, P. J. French, H. K. Gan, M. R. Gilbert, P. V. Gould, M. R. Grimmer, A. Iavarone, A. Ismail, M. D. Jenkinson, M. Khasraw, H. Kim, M. C. M. Kouwenhoven, P. S. Laviolette, M. Li, P. Lichter, K. L. Ligon, A. K. Lowman, T. M. Malta, T. Mazor, K. L. McDonald, A. M. Molinaro, D. H. Nam, N. Nayyar, H. K. Ng, C. Y. Ngan, S. P. Niclou, J. M. Niers, H. Noushmehr, J. Noorbakhsh, D. R. Ormond, C. K. Park, L. M. Poisson, R. Rabadan, B. Radlwimmer, G. Rao, G. Reifenberger, J. K. Sa, M. Schuster, B. L. Shaw, S. C. Short, P. A. Sillevis Smitt, A. E. Sloan, M. Smits, H. Suzuki, G. Tabatabai, E. G. Van Meir, C. Watts, M. Weller, P. Wesseling, B. A. Westerman, G. Widhalm, A. Woehrer, W. K. A. Yung, G. Zadeh, J. T. Huse, J. F. de Groot, L. F. Stead, R. G. W. Verhaak; The GLASS Consortium, Longitudinal molecular trajectories of diffuse glioma in adults. *Nature* **576**, 112–120 (2019).

18. R. B. Puchalski, N. Shah, J. Miller, R. Dalley, S. R. Nomura, J. G. Yoon, K. A. Smith, M. Lankerovich, D. Bertagnolli, K. Bickley, A. F. Boe, K. Brouner, S. Butler, S. Caldejon, M. Chapin, S. Datta, N. Dee, T. Desta, T. Dolbeare, N. Dotson, A. Ebbert, D. Feng, X. Feng, M. Fisher, G. Gee, J. Goldy, L. Gourley, B. W. Gregor, G. Gu, N. Hejazinia, J. Hohmann, P. Hothi, R. Howard, K. Joines, A. Kriedberg, L. Kuan, C. Lau, F. Lee, H. Lee, T. Lemon, F. Long, N. Mastan, E. Mott, C. Murthy, K. Ngo, E. Olson, M. Reding, Z. Riley, D. Rosen, D. Sandman, N. Shapovalova, C. R. Slaughterbeck, A. Sodt, G. Stockdale, A. Szafer, W. Wakeman, P. E. Wohnoutka, S. J. White, D. Marsh, R. C. Rostomily, L. Ng, C. Dang, A. Jones, B. Keogh, H. R. Gittleman, J. S. Barnholtz-Sloan, P. J. Cimino, M. S. Uppin, C. Dirk Keene, F. R. Farrokhi, J. D.

Lathia, M. E. Berens, A. Iavarone, A. Bernard, E. Lein, J. W. Phillips, S. W. Rostad, C. Cobbs, M. J. Hawrylycz, G. D. Foltz, An anatomic transcriptional atlas of human glioblastoma. *Science* **360**, 660–663 (2018).

19. B. J. Gill, D. J. Pisapia, H. R. Malone, H. Goldstein, L. Lei, A. Sonabend, J. Yun, J. Samanamud, J. S. Sims, M. Banu, A. Dovas, A. F. Teich, S. A. Sheth, G. M. McKhann, M. B. Sisti, J. N. Bruce, P. A. Sims, P. Canoll, MRI-localized biopsies reveal subtype-specific differences in molecular and cellular composition at the margins of glioblastoma. *Proc. Natl. Acad. Sci. U.S.A.* **111**, 12550–12555 (2014).

20. V. Venkataramani, Y. Yang, M. C. Schubert, E. Reyhan, S. K. Tetzlaff, N. Wißmann, M. Botz, S. J. Soyka, C. A. Beretta, R. L. Pramatarov, L. Fankhauser, L. Garofano, A. Freudenberg, J. Wagner, D. I. Tanev, M. Ratliff, R. Xie, T. Kessler, D. C. Hoffmann, L. Hai, Y. Dörflinger, S. Hoppe, Y. A. Yabo, A. Golebiewska, S. P. Niclou, F. Sahm, A. Lasorella, M. Slowik, L. Döring, A. Iavarone, W. Wick, T. Kuner, F. Winkler, Glioblastoma hijacks neuronal mechanisms for brain invasion. *Cell* **185**, 2899–2917.e31 (2022).

21. R. G. W. Verhaak, K. A. Hoadley, E. Purdom, V. Wang, Y. Qi, M. D. Wilkerson, C. R. Miller, L. Ding, T. Golub, J. P. Mesirov, G. Alexe, M. Lawrence, M. O'Kelly, P. Tamayo, B. A. Weir, S. Gabriel, W. Winckler, S. Gupta, L. Jakkula, H. S. Feiler, J. G. Hodgson, C. D. James, J. N. Sarkaria, C. Brennan, A. Kahn, P. T. Spellman, R. K. Wilson, T. P. Speed, J. W. Gray, M. Meyerson, G. Getz, C. M. Perou, D. N. Hayes; Cancer Genome Atlas Research Network, Integrated genomic analysis identifies clinically relevant subtypes of glioblastoma characterized by abnormalities in PDGFRA, IDH1, EGFR, and NF1. *Cancer Cell* **17**, 98–110 (2010).

22. C. Neftel, J. Laffy, M. G. Filbin, T. Hara, M. E. Shore, G. J. Rahme, A. R. Richman, D. Silverbush, M. L. Shaw, C. M. Hebert, J. Dewitt, S. Gritsch, E. M. Perez, L. N. Gonzalez Castro, X. Lan, N. Druck, C. Rodman, D. Dionne, A. Kaplan, M. S. Bertalan, J. Small, K. Pelton, S. Becker, D. Bonal, Q. D. Nguyen, R. L. Servis, J. M. Fung, R. Mylvaganam, L. Mayr, J. Gojo, C. Haberler, R. Geyeregger, T. Czech, I. Slavc, B. V. Nahed, W. T. Curry, B. S. Carter, H. Wakimoto, P. K. Brastianos, T. T. Batchelor, A. Stemmer-Rachamimov, M. Martinez-Lage, M. P. Frosch, I. Stamenkovic, N. Riggi, E. Rheinbay, M. Monje, O. Rozenblatt-Rosen, D. P. Cahill,

A. P. Patel, T. Hunter, I. M. Verma, K. L. Ligon, D. N. Louis, A. Regev, B. E. Bernstein, I. Tirosh, M. L. Suvà, An integrative model of cellular states, plasticity, and genetics for glioblastoma. *Cell* **178**, 835–849.e21 (2019).

23. C. P. Couturier, S. Ayyadhury, P. U. Le, J. Nadaf, J. Monlong, G. Riva, R. Allache, S. Baig, X. Yan, M. Bourgey, C. Lee, Y. C. D. Wang, V. Wee Yong, M. C. Guiot, H. Najafabadi, B. Misic, J. Antel, G. Bourque, J. Ragoussis, K. Petrecca, Single-cell RNA-seq reveals that glioblastoma recapitulates a normal neurodevelopmental hierarchy. *Nat. Commun.* **11**, 3406 (2020).

24. L. Garofano, S. Migliozzi, Y. T. Oh, F. D'Angelo, R. D. Najac, A. Ko, B. Frangaj, F. P. Caruso, K. Yu, J. Z. Yuan, W. T. Zhao, A. L. Di Stefano, F. Bielle, T. Jiang, P. Sims, M. L. Suva, F. C. Tang, X. D. Su, M. Ceccarelli, M. Sanson, A. Lasorella, A. Iavarone, Pathway-based classification of glioblastoma uncovers a mitochondrial subtype with therapeutic vulnerabilities. *Nat. Cancer* **2**, 141–156 (2021).

25. L. M. Richards, O. K. N. Whitley, G. MacLeod, F. M. G. Cavalli, F. J. Coutinho, J. E. Jaramillo, N. Svergun, M. Riverin, D. C. Croucher, M. Kushida, K. Yu, P. Guilhamon, N. Rastegar, M. Ahmadi, J. K. Bhatti, D. A. Bozek, N. Li, L. Lee, C. Che, E. Luis, N. I. Park, Z. Xu, T. Ketela, R. A. Moore, M. A. Marra, J. Spears, M. D. Cusimano, S. Das, M. Bernstein, B. Haibe-Kains, M. Lupien, H. A. Luchman, S. Weiss, S. Angers, P. B. Dirks, G. D. Bader, T. J. Pugh, Gradient of developmental and injury response transcriptional states defines functional vulnerabilities underpinning glioblastoma heterogeneity. *Nat. Cancer* **2**, 157–173 (2021).

26. L. Wang, H. Babikir, S. Müller, G. Yagnik, K. Shamardani, F. Catalan, G. Kohanbash, B. Alvarado, E. Di Lullo, A. Kriegstein, S. Shah, H. Wadhwa, S. M. Chang, J. J. Phillips, M. K. Aghi, A. A. Diaz, The phenotypes of proliferating glioblastoma cells reside on a single axis of variation. *Cancer Discov.* **9**, 1708–1719 (2019).

27. X. Wang, Q. Sun, W. Wang, B. Liu, Y. Gu, L. Chen, Decoding key cell sub-populations and molecular alterations in glioblastoma at recurrence by single-cell analysis. *Acta Neuropathol. Commun.* **11**, 125 (2023).

28. A. P. Patel, I. Tirosh, J. J. Trombetta, A. K. Shalek, S. M. Gillespie, H. Wakimoto, D. P. Cahill, B. V. Nahed, W. T. Curry, R. L. Martuza, D. N. Louis, O. Rozenblatt-Rosen, M. L. Suvà, A. Regev, B. E. Bernstein, Single-cell RNA-seq highlights intratumoral heterogeneity in primary glioblastoma. *Science* **344**, 1396–1401 (2014).

29. P. Guilhamon, C. Chesnelong, M. M. Kushida, A. Nikolic, D. Singhal, G. MacLeod, S. A. Madani Tonekaboni, F. M. Cavalli, C. Arlidge, N. Rajakulendran, N. Rastegar, X. Hao, R. Hassam, L. J. Smith, H. Whetstone, F. J. Coutinho, B. Nadorp, K. I. Ellestad, H. A. Luchman, J. A. Chan, M. S. Shoichet, M. D. Taylor, B. Haibe-Kains, S. Weiss, S. Angers, M. Gallo, P. B. Dirks, M. Lupien, Single-cell chromatin accessibility profiling of glioblastoma identifies an invasive cancer stem cell population associated with lower survival. *eLife* **10**, e64090 (2021).

30. K. C. Johnson, K. J. Anderson, E. T. Courtois, A. D. Gujar, F. P. Barthel, F. S. Varn, D. Luo, M. Seignon, E. Yi, H. Kim, M. R. H. Estecio, D. Zhao, M. Tang, N. E. Navin, R. Maurya, C. Y. Ngan, N. Verburg, P. C. de Witt Hamer, K. Bulsara, M. L. Samuels, S. Das, P. Robson, R. G. W. Verhaak, Single-cell multimodal glioma analyses identify epigenetic regulators of cellular plasticity and environmental stress response. *Nat. Genet.* **53**, 1456–1468 (2021).

31. J. G. Nicholson, H. A. Fine, Diffuse glioma heterogeneity and its therapeutic implications. *Cancer Discov.* **11**, 575–590 (2021).

32. C. H.Waddington, *The Strategy of the Genes* (Routledge, 1957), 262 pp. .

33. W. A. Flavahan, E. Gaskell, B. E. Bernstein, Epigenetic plasticity and the hallmarks of cancer. *Science* **357**, eaal2380 (2017).

34. L. Zhu, P. Yang, Y. Zhao, Z. Zhuang, Z. Wang, R. Song, J. Zhang, C. Liu, Q. Gao, Q. Xu, X. Wei, H. Sun, B. Ye, Y. Wu, N. Zhang, G. Lei, L. Yu, J. Yan, G. Diao, F. Meng, C. Bai, P. Mao, Y. Yu, M. Wang, Y. Yuan, Q. Deng, Z. Li, Y. Huang, G. Hu, Y. Liu, X. Wang, Z. Xu, P. Liu, Y. Bi, Y. Shi, S. Zhang, Z. Chen, J. Wang, X. Xu, G. Wu, F. Wang, G. Gao, L. Liu, W. Liu, Single-cell sequencing of peripheral mononuclear cells reveals distinct immune response landscapes of COVID-19 and influenza patients. *Immunity* **53**, 685–696.e3 (2020).

35. A. Nikolic, D. Singhal, K. Ellestad, M. Johnston, Y. Shen, A. Gillmor, S. Morrissy, J. G. Cairncross, S. Jones, M. Lupien, J. A. Chan, P. Neri, N. Bahlis, M. Gallo, Copy-scAT: Deconvoluting single-cell chromatin accessibility of genetic subclones in cancer. *Sci. Adv.* **7**, eabg6045 (2021).

36. C. P. Couturier, J. Nadaf, Z. Li, S. Baig, G. Riva, P. Le, D. J. Kloosterman, J. Monlong, A. Nkili Meyong, R. Allache, T. Degenhard, M. Al-Rashid, M. C. Guiot, G. Bourque, J. Ragoussis, L. Akkari, F. J. Quintana, K. Petrecca, Glioblastoma scRNA-seq shows treatment-induced, immune-dependent increase in mesenchymal cancer cells and structural variants in distal neural stem cells. *Neuro Oncol.* **24**, 1494–1508 (2022).

37. J. E. Moore, M. J. Purcaro, H. E. Pratt, C. B. Epstein, N. Shoresh, J. Adrian, T. Kawli, C. A. Davis, A. Dobin, R. Kaul, J. Halow, E. L. Van Nostrand, P. Freese, D. U. Gorkin, Y. Shen, Y. He, M. Mackiewicz, F. Pauli-Behn, B. A. Williams, A. Mortazavi, C. A. Keller, X. O. Zhang, S. I. Elhajjajy, J. Huey, D. E. Dickel, V. Snetkova, X. Wei, X. Wang, J. C. Rivera-Mulia, J. Rozowsky, J. Zhang, S. B. Chhetri, J. Zhang, A. Victorsen, K. P. White, A. Visel, G. W. Yeo, C. B. Burge, E. Lécuyer, D. M. Gilbert, J. Dekker, J. Rinn, E. M. Mendenhall, J. R. Ecker, M. Kellis, R. J. Klein, W. S. Noble, A. Kundaje, R. Guigó, P. J. Farnham, J. M. Cherry, R. M. Myers, B. Ren, B. R. Graveley, M. B. Gerstein, L. A. Pennacchio, M. P. Snyder, B. E. Bernstein, B. Wold, R. C. Hardison, T. R. Gingeras, J. A. Stamatoyannopoulos, Z. Weng, Expanded encyclopaedias of DNA elements in the human and mouse genomes. *Nature* **583**, 699–710 (2020).

38. R. Andersson, C. Gebhard, I. Miguel-Escalada, I. Hoof, J. Bornholdt, M. Boyd, Y. Chen, X. Zhao, C. Schmidl, T. Suzuki, E. Ntini, E. Arner, E. Valen, K. Li, L. Schwarzfischer, D. Glatz, J. Raithel, B. Lilje, N. Rapin, F. O. Bagger, M. Jørgensen, P. R. Andersen, N. Bertin, O. Rackham, A. M. Burroughs, J. K. Baillie, Y. Ishizu, Y. Shimizu, E. Furuhata, S. Maeda, Y. Negishi, C. J. Mungall, T. F. Meehan, T. Lassmann, M. Itoh, H. Kawaji, N. Kondo, J. Kawai, A. Lennartsson, C. O. Daub, P. Heutink, D. A. Hume, T. H. Jensen, H. Suzuki, Y. Hayashizaki, F. Müller, A. R. R. Forrest, P. Carninci, M. Rehli, A. Sandelin, An atlas of active enhancers across human cell types and tissues. *Nature* **507**, 455–461 (2014).

39. I. Yanai, H. Benjamin, M. Shmoish, V. Chalifa-Caspi, M. Shklar, R. Ophir, A. Bar-Even, S. Horn-Saban, M. Safran, E. Domany, D. Lancet, O. Shmueli, Genome-wide midrange transcription profiles reveal expression level relationships in human tissue specification. *Bioinformatics* **21**, 650–659 (2005).

40. C. Y. McLean, D. Bristor, M. Hiller, S. L. Clarke, B. T. Schaar, C. B. Lowe, A. M. Wenger, G. Bejerano, GREAT improves functional interpretation of cis-regulatory regions. *Nat. Biotechnol* **28**, 495–501 (2010).

41. J. Wang, J. Wang, L. Yang, C. Zhao, L. N. Wu, L. Xu, F. Zhang, Q. Weng, M. Wegner, Q. R. Lu, CTCF-mediated chromatin looping in EGR2 regulation and SUZ12 recruitment critical for peripheral myelination and repair. *Nat. Commun.* **11**, 4133 (2020).

42. R. Mizuguchi, S. Kriks, R. Cordes, A. Gossler, Q. Ma, M. Goulding, Ascl1 and Gsh1/2 control inhibitory and excitatory cell fate in spinal sensory interneurons. *Nat. Neurosci.* **9**, 770–778 (2006).

43. A. Maiques-Diaz, G. J. Spencer, J. T. Lynch, F. Ciceri, E. L. Williams, F. M. R. Amaral, D. H. Wiseman, W. J. Harris, Y. Li, S. Sahoo, J. R. Hitchin, D. P. Mould, E. E. Fairweather, B. Waszkowycz, A. M. Jordan, D. L. Smith, T. C. P. Somervaille, Enhancer activation by pharmacologic displacement of LSD1 from GFI1 induces differentiation in acute myeloid leukemia. *Cell Rep.* **22**, 3641–3659 (2018).

44. S. M. Glasgow, J. C. Carlson, W. Zhu, L. S. Chaboub, P. Kang, H. K. Lee, Y. M. Clovis, B. E. Lozzi, R. J. McEvilly, M. G. Rosenfeld, C. J. Creighton, S. K. Lee, C. A. Mohila, B. Deneen, Glia-specific enhancers and chromatin structure regulate NFIA expression and glioma tumorigenesis. *Nat Neurosci.* **20**, 1520–1528 (2017).

45. J. Lee, E. Hoxha, H. R. Song, A novel NFIA-NFκB feed-forward loop contributes to glioblastoma cell survival. *Neuro Oncol.* **19**, 524–534 (2017).

46. R. Raviram, A. Raman, S. Preissl, J. Ning, S. Wu, T. Koga, K. Zhang, C. W. Brennan, C. Zhu, J. Luebeck, K. Van Deynze, J. Y. Han, X. Hou, Z. Ye, A. K. Mischel, Y. E. Li, R. Fang, T.

Baback, J. Mugford, C. Z. Han, C. K. Glass, C. L. Barr, P. S. Mischel, V. Bafna, L. Escoubet, B. Ren, C. C. Chen, Integrated analysis of single-cell chromatin state and transcriptome identified common vulnerability despite glioblastoma heterogeneity. *Proc. Natl. Acad. Sci. U.S.A.* **120**, e2210991120 (2023).

47. S. Kurtenbach, A. M. Cruz, D. A. Rodriguez, M. A. Durante, J. W. Harbour, Uphyloplot2: Visualizing phylogenetic trees from single-cell RNA-seq data. *BMC Genomics* **22**, 419 (2021).

48. A. Bhaduri, E. Di Lullo, D. Jung, S. Muller, E. E. Crouch, C. S. Espinosa, T. Ozawa, B. Alvarado, J. Spatazza, C. R. Cadwell, G. Wilkins, D. Velmeshev, S. J. Liu, M. Malatesta, M. G. Andrews, M. A. Mostajo-Radji, E. J. Huang, T. J. Nowakowski, D. A. Lim, A. Diaz, D. R. Raleigh, A. R. Kriegstein, Outer radial glia-like cancer stem cells contribute to heterogeneity of glioblastoma. *Cell Stem Cell* **26**, 48–63.e6 (2020).

49. L. Wu, W. Wu, J. Zhang, Z. Zhao, L. Li, M. Zhu, M. Wu, F. Wu, F. Zhou, Y. Du, R.-C. Chai, W. Zhang, X. Qiu, Q. Liu, Z. Wang, J. Li, K. Li, A. Chen, Y. Jiang, X. Xiao, H. Zou, R. Srivastava, T. Zhang, Y. Cai, Y. Liang, B. Huang, R. Zhang, F. Lin, L. Hu, X. Wang, X. Qian, S. Lv, B. Hu, S. Zheng, Z. Hu, H. Shen, Y. You, R. G. W. Verhaak, T. Jiang, Q. Wang, Natural coevolution of tumor and immunoenvironment in glioblastoma. *Cancer Discov.* **12**, 2820–2837 (2022).

50. S. Q. Lv, Z. Fu, L. Yang, Q. R. Li, J. Zhu, Q. J. Gai, M. Mao, J. He, Y. Qin, X. X. Yao, X. Lan, Y. X. Wang, H. M. Lu, Y. Xiang, Z. X. Zhang, G. H. Huang, W. Yang, P. Kang, Z. Sun, Y. Shi, X. H. Yao, X. W. Bian, Y. Wang, Comprehensive omics analyses profile genesets related with tumor heterogeneity of multifocal glioblastomas and reveal LIF/CCL2 as biomarkers for mesenchymal subtype. *Theranostics* **12**, 459–473 (2022).

51. G. S. Kinker, A. C. Greenwald, R. Tal, Z. Orlova, M. S. Cuoco, J. M. McFarland, A. Warren, C. Rodman, J. A. Roth, S. A. Bender, B. Kumar, J. W. Rocco, P. Fernandes, C. C. Mader, H. Keren-Shaul, A. Plotnikov, H. Barr, A. Tsherniak, O. Rozenblatt-Rosen, V. Krizhanovsky, S. V. Puram, A. Regev, I. Tirosh, Pan-cancer single-cell RNA-seq identifies recurring programs of cellular heterogeneity. *Nat. Genet.* **52**, 1208–1218 (2020).

52. Q. Wang, B. Hu, X. Hu, H. Kim, M. Squatrito, L. Scarpace, A. C. de Carvalho, S. Lyu, P. Li, Y. Li, F. Barthel, H. J. Cho, Y. H. Lin, N. Satani, E. Martinez-Ledesma, S. Zheng, E. Chang, C. E. G. Sauvé, A. Olar, Z. D. Lan, G. Finocchiaro, J. J. Phillips, M. S. Berger, K. R. Gabrusiewicz, G. Wang, E. Eskilsson, J. Hu, T. Mikkelsen, R. A. DePinho, F. Muller, A. B. Heimberger, E. P. Sulman, D. H. Nam, R. G. W. Verhaak, Tumor evolution of glioma-intrinsic gene expression subtypes associates with immunological changes in the microenvironment. *Cancer Cell* **32**, 42–56.e46 (2017).

53. D. Szklarczyk, A. L. Gable, D. Lyon, A. Junge, S. Wyder, J. Huerta-Cepas, M. Simonovic, N. T. Doncheva, J. H. Morris, P. Bork, L. J. Jensen, C. von Mering, STRING v11: Protein-protein association networks with increased coverage, supporting functional discovery in genome-wide experimental datasets. *Nucleic Acids Res.* **47**, D607–D613 (2019).

54. Y. A. Yabo, S. P. Niclou, A. Golebiewska, Cancer cell heterogeneity and plasticity: A paradigm shift in glioblastoma. *Neuro Oncol.* **24**, 669–682 (2022).

55. S. Heuer, F. Winkler, Glioblastoma revisited: From neuronal-like invasion to pacemaking. *Trends Cancer* **9**, 887–896 (2023).

56. L. J. Brooks, H. S. Ragdale, C. S. Hill, M. Clements, S. Parrinello, Injury programs shape glioblastoma. *Trends Neurosci.* **45**, 865–876 (2022).

57. A. Dirkse, A. Golebiewska, T. Buder, P. V. Nazarov, A. Muller, S. Poovathingal, N. H. Brons, S. Leite, N. Sauvageot, D. Sarkisjan, M. Seyfrid, S. Fritah, D. Stieber, A. Michelucci, F. Hertel, C. Herold-Mende, F. Azuaje, A. Skupin, R. Bjerkvig, A. Deutsch, A. Voss-Bohme, S. P. Niclou, Stem cell-associated heterogeneity in glioblastoma results from intrinsic tumor plasticity shaped by the microenvironment. *Nat. Commun.* **10**, 1787 (2019).

58. C. Lee, V. A. Rudneva, S. Erkek, M. Zapatka, L. Q. Chau, S. K. Tacheva-Grigorova, A. Garancher, J. M. Rusert, O. Aksoy, R. Lea, H. P. Mohammad, J. Wang, W. A. Weiss, H. L. Grimes, S. M. Pfister, P. A. Northcott, R. J. Wechsler-Reya, Lsd1 as a therapeutic target in Gfi1-activated medulloblastoma. *Nat. Commun.* **10**, 332 (2019).

59. Y. Peng, P. Zhang, X. Huang, Q. Yan, M. Wu, R. Xie, Y. Wu, M. Zhang, Q. Nan, J. Zhao, A. Li, J. Xiong, Y. Ren, Y. Bai, Y. Chen, S. Liu, J. Wang, Direct regulation of FOXK1 by C-jun promotes proliferation, invasion and metastasis in gastric cancer cells. *Cell Death Dis.* **7**, e2480 (2016).

60. F. Xuan, M. Huang, W. Liu, H. Ding, L. Yang, H. Cui, Homeobox C9 suppresses Beclin1-mediated autophagy in glioblastoma by directly inhibiting the transcription of death-associated protein kinase 1. *Neuro Oncol.* **18**, 819–829 (2016).

61. R. Su, S. Cao, J. Ma, Y. Liu, X. Liu, J. Zheng, J. Chen, L. Liu, H. Cai, Z. Li, L. Zhao, Q. He, Y. Xue, Knockdown of SOX2OT inhibits the malignant biological behaviors of glioblastoma stem cells via up-regulating the expression of miR-194-5p and miR-122. *Mol. Cancer* **16**, 171 (2017).

62. B. Van de Sande, C. Flerin, K. Davie, M. De Waegeneer, G. Hulselmans, S. Aibar, R. Seurinck, W. Saelens, R. Cannoodt, Q. Rouchon, T. Verbeiren, D. De Maeyer, J. Reumers, Y. Saeys, S. Aerts, A scalable SCENIC workflow for single-cell gene regulatory network analysis. *Nat. Protoc.* **15**, 2247–2276 (2020).

63. ENCODE Project Consortium, An integrated encyclopedia of DNA elements in the human genome. *Nature* **489**, 57–74 (2012).

64. X. Wang, R. Zhou, Y. Xiong, L. Zhou, X. Yan, M. Wang, F. Li, C. Xie, Y. Zhang, Z. Huang, C. Ding, K. Shi, W. Li, Y. Liu, Z. Cao, Z. N. Zhang, S. Zhou, C. Chen, Y. Zhang, L. Chen, Y. Wang, Sequential fate-switches in stem-like cells drive the tumorigenic trajectory from human neural stem cells to malignant glioma. *Cell Res.* **31**, 684–702 (2021).

65. L. Wang, J. Jung, H. Babikir, K. Shamardani, S. Jain, X. Feng, N. Gupta, S. Rosi, S. Chang, D. Raleigh, D. Solomon, J. J. Phillips, A. A. Diaz, A single-cell atlas of glioblastoma evolution under therapy reveals cell-intrinsic and cell-extrinsic therapeutic targets. *Nat. Cancer* **3**, 1534–1552 (2022).

66. Z. Chen, S. Wang, H. L. Li, H. Luo, X. Wu, J. Lu, H. W. Wang, Y. Chen, D. Chen, W. T. Wu, S. Zhang, Q. He, D. Lu, N. Liu, Y. You, W. Wu, H. Wang, FOSL1 promotes proneural-to-

mesenchymal transition of glioblastoma stem cells via UBC9/CYLD/NF-κB axis. *Mol. Ther.* **30**, 2568–2583 (2022).

67. C. Marques, T. Unterkircher, P. Kroon, B. Oldrini, A. Izzo, Y. Dramaretska, R. Ferrarese, E. Kling, O. Schnell, S. Nelander, E. F. Wagner, L. Bakiri, G. Gargiulo, M. S. Carro, M. Squatrito, NF1 regulates mesenchymal glioblastoma plasticity and aggressiveness through the AP-1 transcription factor FOSL1. *eLife* **10**, e64846 (2021).

68. Z. Tang, B. Kang, C. Li, T. Chen, Z. Zhang, GEPIA2: An enhanced web server for large-scale expression profiling and interactive analysis. *Nucleic Acids Res.* **47**, W556–W560 (2019).

69. Cancer Genome Atlas Research Network, J. N. Weinstein, E. A. Collisson, G. B. Mills, K. R. M. Shaw, B. A. Ozenberger, K. Ellrott, I. Shmulevich, C. Sander, J. M. Stuart, The Cancer Genome Atlas Pan-Cancer analysis project. *Nat. Genet.* **45**, 1113–1120 (2013).

70. J. Lonsdale, J. Thomas, M. Salvatore, R. Phillips, E. Lo, S. Shad, R. Hasz, G. Walters, F. Garcia, N. Young, B. Foster, M. Moser, E. Karasik, B. Gillard, K. Ramsey, S. Sullivan, J. Bridge, H. Magazine, J. Syron, J. Fleming, L. Siminoff, H. Traino, M. Mosavel, L. Barker, S. Jewell, D. Rohrer, D. Maxim, D. Filkins, P. Harbach, E. Cortadillo, B. Berghuis, L. Turner, E. Hudson, K. Feenstra, L. Sobin, J. Robb, P. Branton, G. Korzeniewski, C. Shive, D. Tabor, L. Qi, K. Groch, S. Nampally, S. Buia, A. Zimmerman, A. Smith, R. Burges, K. Robinson, K. Valentino, D. Bradbury, M. Cosentino, N. Diaz-Mayoral, M. Kennedy, T. Engel, P. Williams, K. Erickson, K. Ardlie, W. Winckler, G. Getz, D. De Luca, D. M. Arthur, M. Kellis, A. Thomson, T. Young, E. Gelfand, M. Donovan, Y. Meng, G. Grant, D. Mash, Y. Marcus, M. Basile, J. Liu, J. Zhu, Z. Tu, N. J. Cox, D. L. Nicolae, E. R. Gamazon, H. K. Im, A. Konkashbaev, J. Pritchard, M. Stevens, T. Flutre, X. Wen, E. T. Dermitzakis, T. Lappalainen, R. Guigo, J. Monlong, M. Sammeth, D. Koller, A. Battle, S. Mostafavi, M. M. Carthy, M. Rivas, J. Maller, I. Rusyn, A. Nobel, F. Wright, A. Shabalin, M. Feolo, N. Sharopova, A. Sturcke, J. Paschal, J. M. Anderson, E. L. Wilder, L. K. Derr, E. D. Green, J. P. Struewing, G. Temple, S. Volpi, J. T. Boyer, E. J. Thomson, M. S. Guyer, C. Ng, A. Abdallah, D. Colantuoni, T. R. Insel, S. E. Koester, A Roger Little, P. K. Bender, T. Lehner, Y. Yao, C. C. Compton, J. B. Vaught, S. Sawyer, N. C.

Lockhart, J. Demchok, H. F. Moore, The Genotype-Tissue Expression (GTEx) project. *Nat. Genet.* **45**, 580–585 (2013).

71. GTEx Consortium, The Genotype-Tissue Expression (GTEx) pilot analysis: Multitissue gene regulation in humans. *Science* **348**, 648–660 (2015).

72. Z. Sheng, L. Li, L. J. Zhu, T. W. Smith, A. Demers, A. H. Ross, R. P. Moser, M. R. Green, A genome-wide RNA interference screen reveals an essential CREB3L2-ATF5-MCL1 survival pathway in malignant glioma with therapeutic implications. *Nat. Med.* **16**, 671–677 (2010).

73. K. Yachi, M. Tsuda, S. Kohsaka, L. Wang, Y. Oda, S. Tanikawa, Y. Ohba, S. Tanaka, miR-23a promotes invasion of glioblastoma via HOXD10-regulated glial-mesenchymal transition. *Signal Transduct. Target. Ther.* **3**, 33 (2018).

74. A. R. Kumar, A. L. Sarver, B. Wu, J. H. Kersey, Meis1 maintains stemness signature in MLL-AF9 leukemia. *Blood* **115**, 3642–3643 (2010).

75. T. Yokoyama, M. Nakatake, T. Kuwata, A. Couzinet, R. Goitsuka, S. Tsutsumi, H. Aburatani, P. J. M. Valk, R. Delwel, T. Nakamura, MEIS1-mediated transactivation of synaptotagmin-like 1 promotes CXCL12/CXCR4 signaling and leukemogenesis. *J. Clin. Invest.* **126**, 1664–1678 (2016).

76. Y.-A. Zhang, Y. Zhou, X. Luo, K. Song, X. Ma, A. Sathe, L. Girard, G. Xiao, A. F. Gazdar, SHOX2 is a potent independent biomarker to predict survival of WHO grade II-III diffuse gliomas. *EBioMedicine* **13**, 80–89 (2016).

77. M. Ahuja, N. Ammal Kaidery, O. C. Attucks, E. McDade, D. M. Hushpulian, A. Gaisin, I. Gaisina, Y. H. Ahn, S. Nikulin, A. Poloznikov, I. Gazaryan, M. Yamamoto, M. Matsumoto, K. Igarashi, S. M. Sharma, B. Thomas, Bach1 derepression is neuroprotective in a mouse model of Parkinson's disease. *Proc. Natl. Acad. Sci. U.S.A.* **118**, e2111643118 (2021).

78. T. Liu, Y. Wang, Y. Wang, S. K. Cheung, P. M. Or, C. W. Wong, J. Guan, Z. Li, W. Yang, Y. Tu, J. Wang, W. L. Ho, H. Gu, A. S. Cheng, S. K. Tsui, A. M. Chan, The mitotic regulator

RCC2 promotes glucose metabolism through BACH1-dependent transcriptional upregulation of hexokinase II in glioma. *Cancer Lett.* **549**, 215914 (2022).

79. Z. Cong, F. Yuan, H. Wang, X. Cai, J. Zhu, T. Tang, L. Zhang, Y. Han, C. Ma, BTB domain and CNC homolog 1 promotes glioma invasion mainly through regulating extracellular matrix and increases ferroptosis sensitivity. *Biochim. Biophys. Acta. Mol. Basis Dis.* **1868**, 166554 (2022).

80. E. Nie, X. Jin, W. Wu, T. Yu, X. Zhou, T. Zhi, Z. Shi, J. Zhang, N. Liu, Y. You, BACH1 promotes temozolomide resistance in glioblastoma through antagonizing the function of p53. *Sci. Rep.* **6**, 39743 (2016).

81. S. Fishilevich, R. Nudel, N. Rappaport, R. Hadar, I. Plaschkes, T. Iny Stein, N. Rosen, A. Kohn, M. Twik, M. Safran, D. Lancet, D. Cohen, GeneHancer: Genome-wide integration of enhancers and target genes in GeneCards. *Database* **2017**, bax028 (2017).

82. C. Trapnell, D. Cacchiarelli, J. Grimsby, P. Pokharel, S. Li, M. Morse, N. J. Lennon, K. J. Livak, T. S. Mikkelsen, J. L. Rinn, The dynamics and regulators of cell fate decisions are revealed by pseudotemporal ordering of single cells. *Nat. Biotechnol.* **32**, 381–386 (2014).

83. V. Bergen, M. Lange, S. Peidli, F. A. Wolf, F. J. Theis, Generalizing RNA velocity to transient cell states through dynamical modeling. *Nat. Biotechnol.* **38**, 1408–1414 (2020).

84. K. Yu, Y. Q. Hu, F. Wu, Q. F. Guo, Z. H. Qian, W. E. Hu, J. Chen, K. Y. Wang, X. Y. Fan, X. L. Wu, J. E. J. Rasko, X. L. Fan, A. Iavarone, T. Jiang, F. C. Tang, X.-D. Su, Surveying brain tumor heterogeneity by single-cell RNA-sequencing of multi-sector biopsies. *Natl. Sci. Rev.* **7**, 1306–1318 (2020).

85. I. Smalley, K. S. M. Smalley, ERK inhibition: A new front in the war against MAPK pathway-driven cancers? *Cancer Discov.* **8**, 140–142 (2018).

86. R. J. Sullivan, J. R. Infante, F. Janku, D. J. L. Wong, J. A. Sosman, V. Keedy, M. R. Patel, G. I. Shapiro, J. W. Mier, A. W. Tolcher, A. Wang-Gillam, M. Sznol, K. Flaherty, E. Buchbinder, R. D. Carvajal, A. M. Varghese, M. E. Lacouture, A. Ribas, S. P. Patel, G. A. DeCrescenzo, C. M.

Emery, A. L. Groover, S. Saha, M. Varterasian, D. J. Welsch, D. M. Hyman, B. T. Li, First-in-class ERK1/2 inhibitor ulixertinib (BVD-523) in patients with MAPK mutant advanced solid tumors: Results of a phase I dose-escalation and expansion study. *Cancer Discov.* **8**, 184–195 (2018).

87. R. Sigaud, L. Rösch, C. Gatzweiler, J. Benzel, L. von Soosten, H. Peterziel, F. Selt, S. Najafi, S. Ayhan, X. F. Gerloff, N. Hofmann, I. Büdenbender, L. Schmitt, K. I. Foerster, J. Burhenne, W. E. Haefeli, A. Korshunov, F. Sahm, C. M. van Tilburg, D. T. W. Jones, S. M. Pfister, D. Knoerzer, B. L. Kreider, M. Sauter, K. W. Pajtler, M. Zuckermann, I. Oehme, O. Witt, T. Milde, The first-in-class ERK inhibitor ulixertinib shows promising activity in mitogen-activated protein kinase (MAPK)-driven pediatric low-grade glioma models. *Neuro Oncol.* **25**, 566–579 (2023).

88. Y. Zenke-Kawasaki, Y. Dohi, Y. Katoh, T. Ikura, M. Ikura, T. Asahara, F. Tokunaga, K. Iwai, K. Igarashi, Heme induces ubiquitination and degradation of the transcription factor bach1. *Mol. Cell. Biol.* **27**, 6962–6971 (2007).

89. G. J. Dhar, I. Bossenmaier, Z. J. Petryka, R. Cardinal, C. J. Watson, Effects of hematin in hepatic porphyria. Further studies. *Ann. Intern. Med.* **83**, 20–30 (1975).

90. C. W. Brennan, R. G. Verhaak, A. McKenna, B. Campos, H. Noushmehr, S. R. Salama, S. Zheng, D. Chakravarty, J. Z. Sanborn, S. H. Berman, R. Beroukhim, B. Bernard, C. J. Wu, G. Genovese, I. Shmulevich, J. Barnholtz-Sloan, L. Zou, R. Vegesna, S. A. Shukla, G. Ciriello, W. K. Yung, W. Zhang, C. Sougnez, T. Mikkelsen, K. Aldape, D. D. Bigner, E. G. Van Meir, M. Prados, A. Sloan, K. L. Black, J. Eschbacher, G. Finocchiaro, W. Friedman, D. W. Andrews, A. Guha, M. Iacocca, B. P. O'Neill, G. Foltz, J. Myers, D. J. Weisenberger, R. Penny, R. Kucherlapati, C. M. Perou, D. N. Hayes, R. Gibbs, M. Marra, G. B. Mills, E. Lander, P. Spellman, R. Wilson, C. Sander, J. Weinstein, M. Meyerson, S. Gabriel, P. W. Laird, D. Haussler, G. Getz, L. Chin; TCGA Research. Network, The somatic genomic landscape of glioblastoma. *Cell* **155**, 462–477 (2013).

91. S. Sakthikumar, S. Sakthikumar, A. Roy, L. Haseeb, M. E. Pettersson, E. Sundström, V. D. Marinescu, K. Lindblad-Toh, K. Lindblad-Toh, K. Forsberg-Nilsson, Whole-genome sequencing

of glioblastoma reveals enrichment of non-coding constraint mutations in known and novel genes. *Genome Biol.* **21**, 127 (2020).

92. F. S. Varn, K. C. Johnson, J. Martinek, J. T. Huse, M. P. Nasrallah, P. Wesseling, L. A. D. Cooper, T. M. Malta, T. E. Wade, T. S. Sabedot, D. Brat, P. V. Gould, A. Wöehrer, K. Aldape, A. Ismail, S. K. Sivajothi, F. P. Barthel, H. Kim, E. Kocakavuk, N. Ahmed, K. White, I. Datta, H. E. Moon, S. Pollock, C. Goldfarb, G. H. Lee, L. Garofano, K. J. Anderson, D. Nehar-Belaid, J. S. Barnholtz-Sloan, S. Bakas, A. T. Byrne, F. D'Angelo, H. K. Gan, M. Khasraw, S. Migliozzi, D. R. Ormond, S. H. Paek, E. G. Van Meir, A. M. E. Walenkamp, C. Watts, T. Weiss, M. Weller, K. Palucka, L. F. Stead, L. M. Poisson, H. Noushmehr, A. Iavarone, R. G. W. Verhaak, D. Ryan Ormond, S. Ha Paek, K. D. Alfaro, S. B. Amin, D. M. Ashley, C. Bock, A. Brodbelt, K. R. Bulsara, A. V. Castro, J. M. Connelly, J. F. Costello, J. F. de Groot, G. Finocchiaro, P. J. French, A. Golebiewska, A. C. Hau, C. Hong, C. Horbinski, K. S. Kannan, M. C. Kouwenhoven, A. Lasorella, P. S. LaViolette, K. L. Ligon, A. K. Lowman, S. Mehta, H. Miletic, A. M. Molinaro, H. K. Ng, S. P. Niclou, J. M. Niers, J. J. Phillips, R. Rabadan, G. Rao, G. Reifenberger, N. Sanai, S. C. Short, P. Sillevis Smitt, A. E. Sloan, M. Smits, J. M. Snyder, H. Suzuki, G. Tabatabai, G. Tanner, W. H. Tomaszewski, M. Wells, B. A. Westerman, H. Wheeler, J. Xie, W. K. Alfred Yung, G. Zadeh, J. Zhao; GLASS. Consortium, Glioma progression is shaped by genetic evolution and microenvironment interactions. *Cell* **185**, 2184–2199.e16 (2022).

93. L. N. G. Castro, I. Liu, M. Filbin, Characterizing the biology of primary brain tumors and their microenvironment via single-cell profiling methods. *Neuro Oncol.* **25**, 234–247 (2023).

94. Y. Hoogstrate, K. Draaisma, S. A. Ghisai, L. van Hijfte, N. Barin, I. de Heer, W. Coppieters, T. P. P. van den Bosch, A. Bolleboom, Z. Gao, A. J. P. E. Vincent, L. Karim, M. Deckers, M. J. B. Taphoorn, M. Kerkhof, A. Weyerbrock, M. Sanson, A. Hoeben, S. Lukacova, G. Lombardi, S. Leenstra, M. Hanse, R. E. M. Fleischeuer, C. Watts, N. Angelopoulos, T. Gorlia, V. Golfinopoulos, V. Bours, M. J. van den Bent, P. A. Robe, P. J. French, Transcriptome analysis reveals tumor microenvironment changes in glioblastoma. *Cancer Cell* **41**, 678–692.e7 (2023).

95. S. Bastola, M. S. Pavlyukov, D. Yamashita, S. Ghosh, H. Cho, N. Kagaya, Z. Zhang, M. Minata, Y. Lee, H. Sadahiro, S. Yamaguchi, S. Komarova, E. Yang, J. Markert, L. B. Nabors, K. Bhat, J. Lee, Q. Chen, D. K. Crossman, K. Shin-Ya, D. H. Nam, I. Nakano, Glioma-initiating cells at tumor edge gain signals from tumor core cells to promote their malignancy. *Nat. Commun.* **11**, 4660 (2020).

96. P. Schmassmann, J. Roux, S. Dettling, S. Hogan, T. Shekarian, T. A. Martins, M. F. Ritz, S. Herter, M. Bacac, G. Hutter, Single-cell characterization of human GBM reveals regional differences in tumor-infiltrating leukocyte activation. *eLife* **12**, RP92678 (2023).

97. V. M. Ravi, P. Will, J. Kueckelhaus, N. Sun, K. Joseph, H. Salie, L. Vollmer, U. Kuliesiute, J. von Ehr, J. K. Benotmane, N. Neidert, M. Follo, F. Scherer, J. M. Goeldner, S. P. Behringer, P. Franco, M. Khiat, J. Zhang, U. G. Hofmann, C. Fung, F. L. Ricklefs, K. Lamszus, M. Boerries, M. Ku, J. Beck, R. Sankowski, M. Schwabenland, M. Prinz, U. Schuller, S. Killmer, B. Bengsch, A. K. Walch, D. Delev, O. Schnell, D. H. Heiland, Spatially resolved multi-omics deciphers bidirectional tumor-host interdependence in glioblastoma. *Cancer Cell* **40**, 639–655.e13 (2022).

98. T. Hara, R. Chanoch-Myers, N. D. Mathewson, C. Myskiw, L. Atta, L. Bussema, S. W. Eichhorn, A. C. Greenwald, G. S. Kinker, C. Rodman, L. N. Gonzalez Castro, H. Wakimoto, O. Rozenblatt-Rosen, X. Zhuang, J. Fan, T. Hunter, I. M. Verma, K. W. Wucherpfennig, A. Regev, M. L. Suvà, I. Tirosh, Interactions between cancer cells and immune cells drive transitions to mesenchymal-like states in glioblastoma. *Cancer Cell* **39**, 779–792.e11 (2021).

99. N. D. Mathewson, O. Ashenberg, I. Tirosh, S. Gritsch, E. M. Perez, S. Marx, L. Jerby-Arnon, R. Chanoch-Myers, T. Hara, A. R. Richman, Y. Ito, J. Pyrdol, M. Friedrich, K. Schumann, M. J. Poitras, P. C. Gokhale, L. N. Gonzalez Castro, M. E. Shore, C. M. Hebert, B. Shaw, H. L. Cahill, M. Drummond, W. Zhang, O. Olawoyin, H. Wakimoto, O. Rozenblatt-Rosen, P. K. Brastianos, X. S. Liu, P. S. Jones, D. P. Cahill, M. P. Frosch, D. N. Louis, G. J. Freeman, K. L. Ligon, A. Marson, E. A. Chiocca, D. A. Reardon, A. Regev, M. L. Suvà, K. W. Wucherpfennig, Inhibitory CD161 receptor identified in glioma-infiltrating T cells by single-cell analysis. *Cell* **184**, 1281–1298.e26 (2021).

100. C. Garcia-Diaz, A. Poysti, E. Mereu, M. P. Clements, L. J. Brooks, F. Galvez-Cancino, S. P. Castillo, W. H. Tang, G. Beattie, L. Courtot, S. Ruiz, F. Roncaroli, Y. Y. Yuan, S. Marguerat, S. A. Quezada, H. Heyn, S. Parrinello, Glioblastoma cell fate is differentially regulated by the microenvironments of the tumor bulk and infiltrative margin. *Cell Rep.* **42**, 112472 (2023).

101. E. Gangoso, B. Southgate, L. Bradley, S. Rus, F. Galvez-Cancino, N. McGivern, E. Guc, C. A. Kapourani, A. Byron, K. M. Ferguson, N. Alfazema, G. Morrison, V. Grant, C. Blin, I. Sou, M. A. Marques-Torrejon, L. Conde, S. Parrinello, J. Herrero, S. Beck, S. Brandner, P. M. Brennan, P. Bertone, J. W. Pollard, S. A. Quezada, D. Sproul, M. C. Frame, A. Serrels, S. M. Pollard, Glioblastomas acquire myeloid-affiliated transcriptional programs via epigenetic immunoediting to elicit immune evasion. *Cell* **184**, 2454–2470.e26 (2021).

102. M. Osswald, E. Jung, F. Sahm, G. Solecki, V. Venkataramani, J. Blaes, S. Weil, H. Horstmann, B. Wiestler, M. Syed, L. L. Huang, M. Ratliff, K. K. Jazi, F. T. Kurz, T. Schmenger, D. Lemke, M. Gommel, M. Pauli, Y. X. Liao, P. Haring, S. Pusch, V. Herl, C. Steinhauser, D. Krunic, M. Jarahian, H. Miletic, A. S. Berghoff, O. Griesbeck, G. Kalamakis, O. Garaschuk, M. Preusser, S. Weiss, H. K. Liu, S. Heiland, M. Platten, P. E. Huber, T. Kuner, A. von Deimling, W. Wick, F. Winkler, Brain tumour cells interconnect to a functional and resistant network. *Nature* **528**, 93–98 (2015).

103. A. S. Venteicher, I. Tirosh, C. Hebert, K. Yizhak, C. Neftel, M. G. Filbin, V. Hovestadt, L. E. Escalante, M. L. Shaw, C. Rodman, S. M. Gillespie, D. Dionne, C. C. Luo, H. Ravichandran, R. Mylvaganam, C. Mount, M. L. Onozato, B. V. Nahed, H. Wakimoto, W. T. Curry, A. J. Iafrate, M. N. Rivera, M. P. Frosch, T. R. Golub, P. K. Brastianos, G. Getz, A. P. Patel, M. Monje, D. P. Cahill, O. Rozenblatt-Rosen, D. N. Louis, B. E. Bernstein, A. Regev, M. L. Suvà, Decoupling genetics, lineages, and microenvironment in IDH-mutant gliomas by single-cell RNA-seq. *Science* **355**, eaai8478 (2017).

104. H. S. Venkatesh, W. Morishita, A. C. Geraghty, D. Silverbush, S. M. Gillespie, M. Arzt, L. T. Tam, C. Espenel, A. Ponnuswami, L. Ni, P. J. Woo, K. R. Taylor, A. Agarwal, A. Regev, D. Brang, H. Vogel, S. Hervey-Jumper, D. E. Bergles, M. L. Suvà, R. C. Malenka, M. Monje, Electrical and synaptic integration of glioma into neural circuits. *Nature* **573**, 539–545 (2019).

105. X. Dai, L. Ye, H. Li, X. Dong, H. Tian, P. Gao, J. Dong, H. Cheng, Crosstalk between microglia and neural stem cells influences the relapse of glioblastoma in GBM immunological microenvironment. *Clin. Immunol.* **251**, 109333 (2023).

106. S. Krishna, A. Choudhury, M. B. Keough, K. Seo, L. Ni, S. Kakaizada, A. Lee, A. Aabedi, G. Popova, B. Lipkin, C. Cao, C. Nava Gonzales, R. Sudharshan, A. Egladyous, N. Almeida, Y. Zhang, A. M. Molinaro, H. S. Venkatesh, A. G. S. Daniel, K. Shamardani, J. Hyer, E. F. Chang, A. Findlay, J. J. Phillips, S. Nagarajan, D. R. Raleigh, D. Brang, M. Monje, S. L. Hervey-Jumper, Glioblastoma remodelling of human neural circuits decreases survival. *Nature* **617**, 599–607 (2023).

107. H. S. Venkatesh, T. B. Johung, V. Caretti, A. Noll, Y. Tang, S. Nagaraja, E. M. Gibson, C. W. Mount, J. Polepalli, S. S. Mitra, P. J. Woo, R. C. Malenka, H. Vogel, M. Bredel, P. Mallick, M. Monje, Neuronal activity promotes glioma growth through neuroligin-3 secretion. *Cell* **161**, 803–816 (2015).

108. H. S. Venkatesh, L. T. Tam, P. J. Woo, J. Lennon, S. Nagaraja, S. M. Gillespie, J. Ni, D. Y. Duveau, P. J. Morris, J. J. Zhao, C. J. Thomas, M. Monje, Targeting neuronal activity-regulated neuroligin-3 dependency in high-grade glioma. *Nature* **549**, 533–537 (2017).

109. H. A. Fine, Malignant Gliomas: Simplifying the Complexity. *Cancer Discov.* **9**, 1650–1652 (2019).

110. M. Weller, M. van den Bent, M. Preusser, E. Le Rhun, J. C. Tonn, G. Minniti, M. Bendszus, C. Balana, O. Chinot, L. Dirven, P. French, M. E. Hegi, A. S. Jakola, M. Platten, P. Roth, R. Rudà, S. Short, M. Smits, M. J. B. Taphoorn, A. von Deimling, M. Westphal, R. Soffietti, G. Reifenberger, W. Wick, EANO guidelines on the diagnosis and treatment of diffuse gliomas of adulthood. *Nat. Rev. Clin. Oncol.* **18**, 170–186 (2021).

111. R. Chaligne, F. Gaiti, D. Silverbush, J. S. Schiffman, H. R. Weisman, L. Kluegel, S. Gritsch, S. D. Deochand, L. N. G. Castro, A. R. Richman, J. Klughammer, T. Biancalani, C. Muus, C. Sheridan, A. Alonso, F. Izzo, J. Park, O. Rozenblatt-Rosen, A. Regev, M. L. Suva, D. A.

Landau, Epigenetic encoding, heritability and plasticity of glioma transcriptional cell states. *Nat. Genet.* **53**, 1469–1479 (2021).

112. L. Heumos, A. C. Schaar, C. Lance, A. Litinetskaya, F. Drost, L. Zappia, M. D. Lücken, D. C. Strobl, J. Henao, F. Curion; Single-cell Best Practices Consortium, H. B. Schiller, F. J. Theis, Best practices for single-cell analysis across modalities. *Nat. Rev. Genet.* **24**, 550–572 (2023).

113. K. Vandereyken, A. Sifrim, B. Thienpont, T. Voet, Methods and applications for single-cell and spatial multi-omics. *Nat. Rev. Genet.* **24**, 494–515 (2023).

114. M. Ratliff, K. Karimian-Jazi, D. C. Hoffmann, L. Rauschenbach, M. Simon, L. Hai, H. Mandelbaum, M. C. Schubert, T. Kessler, S. Uhlig, D. D. Azorin, E. Jung, M. Osswald, G. Solecki, M. E. Maros, V. Venkataramani, M. Glas, N. Etminan, B. Scheffler, W. Wick, F. Winkler, Individual glioblastoma cells harbor both proliferative and invasive capabilities during tumor progression. *Neuro Oncol.* **25**, 2150–2162 (2023).

115. T. Bakken, R. Hodge, J. Miller, Z. Yao, T. Nguyen, B. Aevermann, E. Barkan, D. Bertagnolli, T. Casper, N. Dee, E. Garren, J. Goldy, L. Graybuck, M. Kroll, R. Lasken, K. Lathia, S. Parry, C. Rimorin, R. Scheuermann, N. Schork, S. Shehata, M. Tieu, J. Phillips, A. Bernard, K. Smith, H. Zeng, E. Lein, B. Tasic, Single-nucleus and single-cell transcriptomes compared in matched cortical cell types. *PLOS ONE* **13**, e0209648 (2018).

116. Y. Yu, X. Wei, Q. Deng, Q. Lan, Y. Guo, L. Han, Y. Yuan, P. Fan, P. Wu, S. Shangguan, Y. Liu, Y. Lai, G. Volpe, M. Esteban, C. Liu, Y. Hou, L. Liu, Single-nucleus chromatin accessibility landscape reveals diversity in regulatory regions across distinct adult rat cortex. *Front. Mol. Neurosci.* **14**, 651355 (2021).

117. Q. Shi, S. Liu, K. Kristiansen, L. Liu, The FASTQ+ format and PISA. *Bioinformatics* **38**, 4639–4642 (2022).

118. A. Dobin, C. A. Davis, F. Schlesinger, J. Drenkow, C. Zaleski, S. Jha, P. Batut, M. Chaisson, T. R. Gingeras, STAR: Ultrafast universal RNA-seq aligner. *Bioinformatics* **29**, 15–21 (2013).

119. A. T. L. Lun, S. Riesenfeld, T. Andrews, T. P. Dao, T. Gomes; participants in the 1st Human Cell Atlas Jamboree, J. C. Marioni, EmptyDrops: Distinguishing cells from empty droplets in droplet-based single-cell RNA sequencing data. *Genome Biol.* **20**, 63 (2019).

120. Y. Hao, S. Hao, E. Andersen-Nissen, W. M. Mauck, 3rd, S. Zheng, A. Butler, M. J. Lee, A. J. Wilk, C. Darby, M. Zager, P. Hoffman, M. Stoeckius, E. Papalexi, E. P. Mimitou, J. Jain, A. Srivastava, T. Stuart, L. M. Fleming, B. Yeung, A. J. Rogers, J. M. McElrath, C. A. Blish, R. Gottardo, P. Smibert, R. Satija, Integrated analysis of multimodal single-cell data. *Cell* **184**, 3573–3587.e29 (2021).

121. C. S. McGinnis, L. M. Murrow, Z. J. Gartner, DoubletFinder: Doublet detection in single-cell RNA sequencing data using artificial nearest neighbors. *Cell Sys.* **8**, 329–337.e4 (2019).

122. L. M. Innes, J. Healy, J. Melville, UMAP: uniform manifold approximation and projection for dimension reduction. arXiv:1802.03426 [stat.ML] (2018).

123. Z. Gu, R. Eils, M. Schlesner, Complex heatmaps reveal patterns and correlations in multidimensional genomic data. *Bioinformatics* **32**, 2847–2849 (2016).

124. T. Wu, E. Hu, S. Xu, M. Chen, P. Guo, Z. Dai, T. Feng, L. Zhou, W. Tang, L. Zhan, X. Fu, S. Liu, X. Bo, G. Yu, clusterProfiler 4.0: A universal enrichment tool for interpreting omics data. *Innovation* **2**, 100141 (2021).

125. G. La Manno, R. Soldatov, A. Zeisel, E. Braun, H. Hochgerner, V. Petukhov, K. Lidschreiber, M. E. Kastriti, P. Lönnerberg, A. Furlan, J. Fan, L. E. Borm, Z. Liu, D. van Bruggen, J. Guo, X. He, R. Barker, E. Sundström, G. Castelo-Branco, P. Cramer, I. Adameyko, S. Linnarsson, P. V. Kharchenko, RNA velocity of single cells. *Nature* **560**, 494–498 (2018).

126. H. Li, Aligning sequence reads, clone sequences and assembly contigs with BWA-MEM. arXiv:1303.3997 [q-bio.GN] (2013).

127. J. M. Granja, M. R. Corces, S. E. Pierce, S. T. Bagdatli, H. Choudhry, H. Y. Chang, W. J. Greenleaf, ArchR is a scalable software package for integrative single-cell chromatin accessibility analysis. *Nat. Genet.* **53**, 403–411 (2021).

128. F. A. Wolf, P. Angerer, F. J. Theis, SCANPY: Large-scale single-cell gene expression data analysis. *Genome Biol.* **19**, 15 (2018).